The Renaissance of Einstein’s Theory of Gravitation

JMEPEG
https://doi.org/10.1007/s11665-026-13900-4

1059-9495/$19.00

ORIGINAL RESEARCH ARTICLE

Novel Analytical and Machine Learning Framework Predicting LPBF Heat Treatment Effects on Inconel™ 718 Hardness

Mohsen Dehghanpour Abyaneh, Raffaella Sesana, MohammadSadegh Javadi, Parviz Narimani, Matteo Crachi, and Antonio Caraviello

Submitted: 18 September 2025 / Revised: 10 March 2026 / Accepted: 4 April 2026

In Laser Powder Bed Fusion, a layer-by-layer melting of metal powder takes place and is specifically suited to high-performance applications in advanced technologies using Inconel™ 718. Vickers hardness (HV20) of the samples was measured as an output variable of the machine learning model after the heat treatment and surface polishing. Particle swarm optimization and genetic algorithm were proposed to define the relationships between the input and output data. The prediction of hardness was then done using five regression models, such as support vector machine, Gaussian process regression (GPR), single-layer and deep-layer artificial neural networks (ANNs), and random tree (RT). A novel technique, rollback, for optimizing output data increased the accuracy metrics. GPR and ANNs performed best in terms of training results. The rollback process was also implemented on the test results. GPR and ANN displayed the best results, with the highest R^2, NSE, and KGE values between 0.97 and 0.99, and the lowest MAPE, MAE, and RMSE on the testing data, which proved them as the best solutions. The Kruskal–Wallis test and Taylor diagram were also used to evaluate model performance.

Keywords hardness, heat treatment, inconel™ 718, laser powder bed fusion (LPBF), machine learning (ML)

1. Introduction

The potential of metal additive manufacturing (AM), particularly laser powder bed fusion (LPBF), to change manufacturing through the ability to produce complex geometries with tailored properties has now been realized to a large extent. Laser power, scanning speed, as well as the hatching distance are the most commonly utilized parameters in optimization of processes. These parameters have effects on volumetric energy density (ED), which determines the mechanical characteristics and surface quality of the parts (Ref 1, 2). ED and the scanning process determine the profile of temperature during the printing process, which determines the hardness of components. These interactions are optimizable using statistical tools and machine learning (ML) algorithms to have better mechanical processes.

The most commonly used nickel alloys when going through LPBF additive manufacturing are Inconel™ 625 and Inconel™ 718 to create aerospace parts. These materials have a high ability to resist corrosive media, intense temperatures, and creep, which is another benefit of them (Ref 3). Because Inconel™ 718 can ensure the finest mechanical performance at high temperatures, it is frequently the ideal option for complex components such as liquid rocket engine components (Ref 4–6). A detailed overview of the use of Inconel™ 718 in the production of aeronautical components is provided in (Ref 7). In the case of Inconel™ 718, heating and cooling methods implemented in the deposition process of LPBF enhance the hardness of AM parts compared to the conventional methods (Ref 8).

The AM process has a large influence on the modeling of structural behaviors because the material mechanical properties determine the estimation of structural behaviors (Ref 9, 10). Hardness measurement is a simple and cost-effective way to estimate mechanical behavior. Hardness is referred to as an extrinsic material feature, which is a measure of the material's resistance to plastic deformation when penetrated using an indenter tool on the surface of components (Ref 6, 11). The hardness tests are either non-destructive or semi-destructive, and the hardness test results would prove to show a linear relationship with the mechanical parameters, such as the yield strength, tensile strength, and the Young's modulus (Ref 12, 13). In (Ref 14), the paper discussed the experimental investigation of the influences of the deposition factors on the

MohsenDehghanpoor Abyaneh, Department of Mechanical and Aerospace Engineering (DIMEAS), Politechnico Di Torino, 10129 Turin, Italy; and TN ITALY, Global Manufacturing Organization, Corso Torino 378, 10064 Pinerolo, Turin, Italy; **Raffaella Sesana** and **Matteo Crachi**, Department of Mechanical and Aerospace Engineering (DIMEAS), Politechnico Di Torino, 10129 Turin, Italy; **MohammadSadegh Javadi**, Department of Mechanical Engineering, Amirkabir University of Technology, 424, Hafez Ave., P.O.B. 158754413, Tehran 15875-4413, Iran; **Parviz Narimani**, School of Mechanical Engineering, College of Engineering, University of Tehran, Tehran, Iran; and **Antonio Caraviello**, Sophia High Tech s.r. l., Via Malatesta 30 A, 80049 Naples, Italy. Contact e-mails: mohsen.dehghanpour@polito.it, javadims@aut.ac.ir, parviz.narimani@ut.ac.ir, and antonio.caraviello@sophiahightech.com.

Published online: 20 April 2026

mechanical hardness and structural properties of Inconel™ 718.

Any mechanical property, such as hardness, is hard to predict, technologically speaking, because of the complex interplay of process parameters (Ref 15). The ML regression models have been highly effective in the response to the challenge because of their ability to effectively use the data to apply a given estimate to a set of specific qualities in an accurate fashion and have been widely engaged to predict metal 3D printing mechanical properties (Ref 16). Such models facilitate optimization of systems to enhance the aspect of printing parts. Most of the predictions deal with only those properties that influence performance, which include hardness, tensile strength, and yield strength (Ref 17). A publication explores the role of ML in predicting mechanical properties in composite materials, like yield strength, ultimate tensile strength, elastic modulus, elongation, hardness, and surface roughness in AM materials and components. It emphasizes the presence of the powerful effect of quality data and the combination of ML models and real-time monitoring systems as the crucial pressure of increasing predictability (Ref 8). Substantial ML studies have been performed on the topic of Mg alloys and have indicated that neural networks (NN), random forests (RF), and gradient-boosting (GB) trees are effective in the prediction of mechanical properties, including ultimate tensile strength, elongation, yield strength, and hardness. The other analysis in steel tubes involved the use of NNs, RF, and gradient-boosting trees to predict yield strength, ultimate tensile strength, and hardness. All of which were very precise and thus indicated the promise of ML in predicting the mechanical properties of process parameters (Ref 18, 19). In recent studies on Friction stir welding (FSW) joints of aluminum alloys, the prediction of mechanical characteristics of various temperature conditions using various ML models, like support vector regression (SVR) and Gaussian process regression (GPR), has been examined. In this direction, the studies can be seen as the embodiment of the transformative contribution that ML can make in terms of material science as a means of enhanced prediction and optimization of mechanical properties (Ref 20). In a review (Ref 21), ML methods of predicting mechanical properties of AM titanium alloys with a particular focus on the influence of processing factors are provided. This study highlights the fact that ML has the potential to transform materials science by making improved designs of materials and making more accurate predictions more straightforward, and shows that these techniques could be potentially applied to the optimization of process parameters accordingly. In addition, Xiong et al. (Ref 22) applied five ML algorithms to predict mechanical properties in steels. Among these, RF regression showed the best predictive performance, again underlining the critical role of feature selection in model accuracy.

In one of the articles on the use of ML, the role of processing parameters in the properties and characteristics of the AM components was considered. MechProNet data incorporate the data about AM processing conditions, machines, materials, and resulting mechanical properties (Ref 23, 24). To predict the mechanical properties of AM metals, the possibility of applying different ML methods and modeling the effects of process parameters was discussed in (Ref 23, 25). Such works also prove that, in this course, there are both challenges and opportunities, and they clarify that it is necessary to consider the quality of data and the interpretability of models. In (Ref 26, 27), publications revealed the potential of ML to predict the mechanical properties of additively manufactured parts, such as the yield strength, ultimate tensile strength, and hardness. Gu et al. (Ref 25) examined the prediction of mechanical parameters in LPBF through ML models, where data quality and model interpretability were marked as significant. The aims of such solutions are to provide quality and reliability of the end-created elements due to merging ML and real-time control systems, and also to optimize the process of manufacturing. Luo et al. (Ref 28) investigated the prediction of the mechanical properties of Ti-6Al-4 V with ML models. Further studies determined the use of support vector machines (SVMs) to forecast in AM, and the importance of data-driven techniques should be mentioned (Ref 29). Researchers have demonstrated the power of ML methods in the process parameters optimization and have pointed out the implementation of data-driven methods, making a particular emphasis on the involvement of ML in the enhancement of process control. The results demonstrate the importance of high-quality data as well as a coherent explanation of the model in order to improve the predictive model accuracy and reliability, and a way to a more efficient and performance-oriented manufacturing process (Ref 30, 31).

Table 1 summarizes the conducted research across five main categories under the Study Focus column, highlighting how each work applies machine-learning techniques within the field of additive manufacturing. The second and third columns specify the alloy or material system investigated and the corresponding additive-manufacturing (AM) process used, providing a clear view of the technological context of each study. The fourth column outlines the machine-learning methods employed, ranging from classical regression models to advanced deep-learning architectures. Finally, the fifth column reports the accuracy metrics used in each study, enabling a direct comparison of model performance and identifying which ML approaches demonstrated the highest predictive capability.

Scopus' database was used to study significant concentrations in the literature. In this database, a total of 71 studies were identified regarding the keywords of LPBF, ML, heat treatment, and hardness. A list of essential keywords for this field of research, the network map, was created using the VOSviewer software version 1.6.20 (Fig. 1a) (Ref 32, 33). Node size shows the frequency of keyword occurrence, while link thickness indicates co-occurrence strength. As shown in Fig. 1(b), related to overlay visualization, many studies have been published from 2023 to the present, and these studies are a current issue. The main focuses and most researched topics in these studies are LPBF, mechanical properties, and the use of machine learning techniques in recent studies.

The use of ML regression models in attempting to predict mechanical and hardness behavior during metal 3D printing, especially of LPBF heat treatment effects on Inconel™ 718 hardness, is promising. In the present study, the analysis is conducted exclusively on the numerical dataset provided in the main published reference (Ref 14). While the original reference concentrated on the experimental behavior of the specimens, it did not investigate the quantitative relationships between input parameters and hardness outputs. In contrast, the current work employs an artificial-intelligence-based numerical framework to uncover these relationships, acknowledging that the underlying physical interactions among LPBF parameters are highly complex and not easily captured through traditional analytical methods. Machine-learning models do not yield a single closed-form equation; instead, they provide a robust predictive

Table 1 The review of literatures in the filed of additive manufacturing and metal 3D printing, that enhanced my machine learning approaches

Study focus	Alloy	Additive-manufacturing style	Key ML technologies	References
ML aided prediction & design of mechanical properties	Magnesium alloys	Not AM (materials design study)	Random Forest, Gradient Boosting, SVR, ANN (common in alloy-design ML papers)	Ref 18
Hardness prediction for HEAs in L-AM	High-entropy alloys	Laser additive manufacturing LPBF / L-PBF	Random Forest Regression, XGBoost, SVR, ANN	Ref 19
Vickers hardness prediction under treatments	D2 tool steel	Not AM	Linear Regression, Random Forest, SVR, ANN	Ref 20
Review of ML in AM of titanium alloys	Titanium alloys	General AM (review)	Not a regression study — survey of ML models (RF, SVR, ANN, GPR, CNN)	Ref 21
Machine learning of mechanical properties of steels regression models	Steels	…	SVR, Random Forest, Gradient Boosting, ANN	Ref 22
ML prediction of mechanical properties in metal AM	Various AM metals	Metal additive manufacturing (AM)	GPR, Random Forest, SVR, ANN	Ref 23
ML for material characterization	General materials	Material characterizationNot AM	Gaussian Process Regression, Kernel Ridge Regression, ANN	Ref 24
Universal predictor for LPBF process maps	Various LPBF alloys	Laser powder bed fusion(LPBF)	Gaussian Process Regression, Kernel Ridge Regression, ANN	Ref 25
Predictive modeling for FDM parts	Polymers (FDM)	Fused deposition modeling (FDM)	Linear Regression, Random Forest, SVR, ANN	Ref 26
ANN-based predictive model for FE analysis	Polymers (FDM)	General AM	ANN	Ref 27
Transfer learning for LPBF Ti-6Al-4 V	Ti-6Al-4 V	Laser powder bed fusion (LPBF)	CNN-based regression, Transfer Learning Regression (ResNet-type models)	Ref 28
Data-driven prediction for AM alloys	AM alloys	General AM	GPR, Bayesian Regression, Random Forest	Ref 29
ML module for tensile response of SLMed Ti-6Al-4 V	Ti-6Al-4 V	Selective laser melting (SLM)	ANN, Random Forest, SVR	Ref 30
Surface roughness prediction for AM Ti-6Al-4 V	Ti-6Al-4 V	General AM	Random Forest, SVR, ANN, Gradient Boosting	Ref 31)

mapping capable of both interpolation and extrapolation, enabling the estimation of new hardness values beyond the original experimental domain.

Based on the reviewed literature, the most frequently implemented machine-learning approaches in additive-manufacturing research include support vector regression, Gaussian process regression, and artificial neural networks, all of which represent standard and well-established models in this domain. These methods are therefore adopted in the present study, complemented by a random tree-based model to broaden the generality of the comparative analysis. In addition to these ML techniques, two non-ML optimization algorithms, genetic algorithms and particle swarm optimization, are examined separately. These algorithms are widely used in manufacturing research for parameter optimization, and their inclusion enables a meaningful comparison between traditional optimization strategies and modern machine-learning models.

2. Material and Methods

2.1 Test Specimen

A design of experiment (DOE) method was devised to assess the hardness characteristics of Inconel^{TM} 718 printed via LPBF, according to (Ref 14). The parameters of the LPBF process affect the density of the material and, therefore, the properties of the material (Ref 34). The ED could be impacted by combining four primary parameters: layer thickness (s), laser power (P), hatch distance (h), and scanning speed (v) (Ref 35) (Fig. 2). ED, a parameter associated with material density, porosity, and the mechanism of forming the defects, measures the amount of energy that is given by unit volume of the powder placed. It has the following definition in Eq 1 and is measured in (J/mm3).

$$\mathrm{ED} = \frac{P}{v.s.h} \qquad \text{(Eq 1)}$$

A similar parameter is suggested in (Ref 36), where an experimental investigation into the relationship between ED and surface roughness, pore size and number, and Vickers hardness is described. This parameter is specifically mentioned when the study addresses multiple process parameters concurrently. The test plan, described in (Ref 14), examines the effects of scanning speed and laser power. The processing parameters investigated in the testing plan are based on the nominal parameters supplied by the printer supplier (for Inconel^{TM} 718: P=192W and v=600 mm/s). The greater scope of ED variance is investigated in (Ref 36).

The arrangement of the specimens on the printing platform was designed to assess its impact on the material's hardness and response to seven distinct energy densities. Both deposition and growth planes were evaluated, and each specimen's hardness was measured. Micrography analysis was carried out as well. It was analyzed on as-built and heat-treated specimens to determine how a standard thermal treatment affects them.

In (Ref 14), a detailed description of this experimental campaign is reported. The choice to go for a 30 micron layer is due to the fact that the DOE was originally done to achieve a good roughness quality in order to match the requirements of space hardware. To shorten the discussion, the reader is referred to the reference (Ref 14). Table 2 describes the specific process

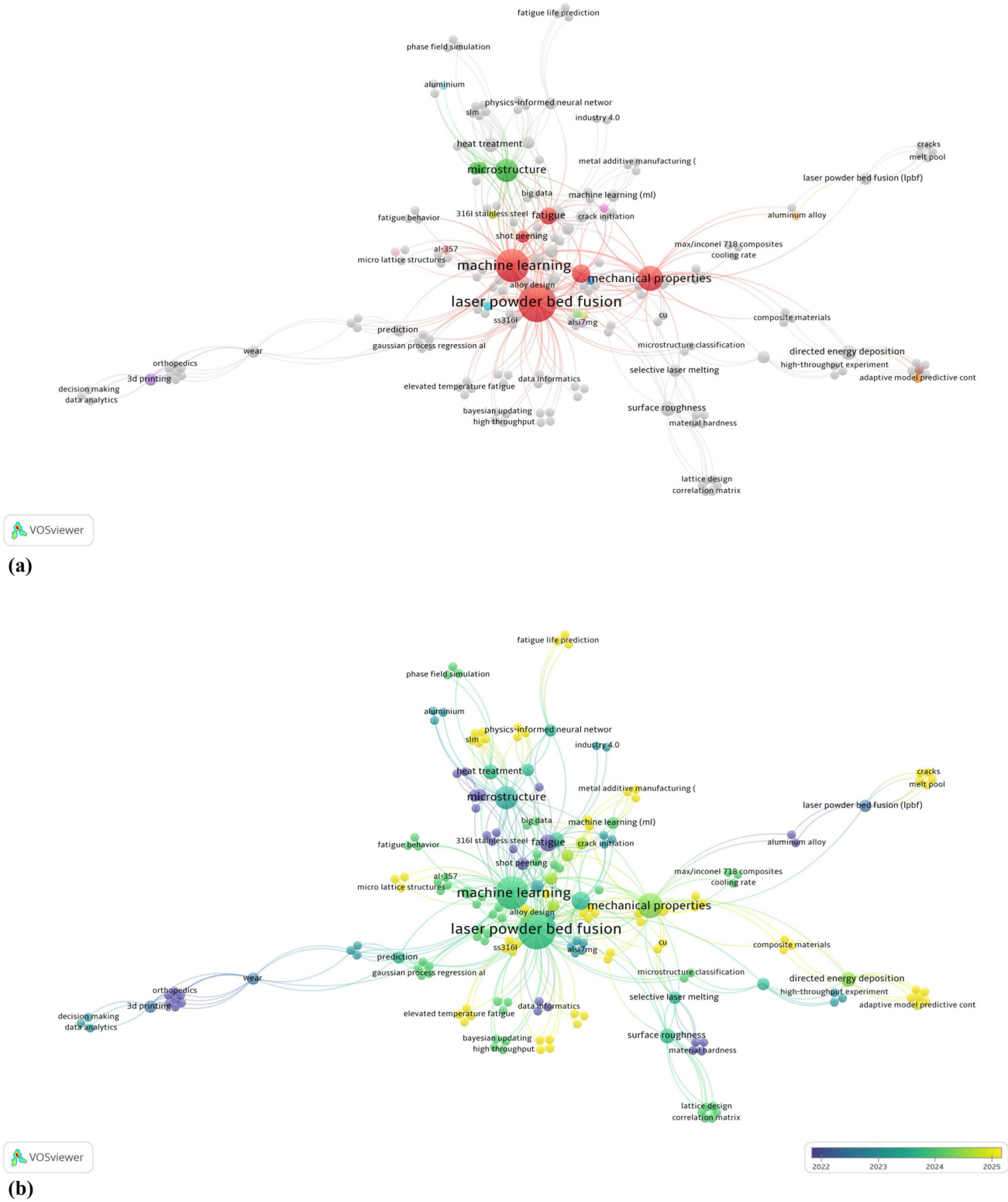

Fig. 1 VOSviewer graphs in this study (a) keyword co-occurrence, (b) time overlay

factors that regulate the internal and external geometry of the component. Additionally, Table 3 indicates the testing parameters, encompassing laser power (P), scanning speed (v), and ED.

2.2 Dataset Evaluation

Twenty-eight cubical specimens were printed in a Concept Laser M2 Series printer (Ref 37), using Inconel™ 718 powder by Sophia High Tech (Napoli, Italy). The chosen powder,

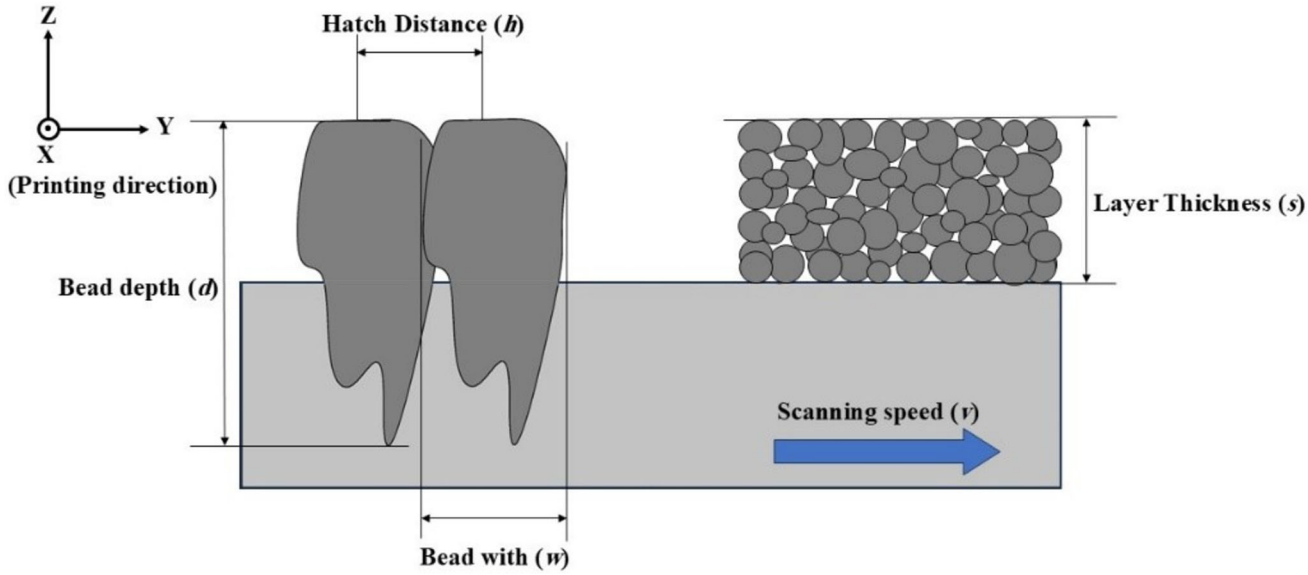

Fig. 2 The schematic representation of ED parameters

Table 2 Main body and contour process parameters (14). R. Sesana, C. Delprete, M. Pizzarelli, M. Crachi, L. Lavagna, D. Borrelli, and A. Caraviello. © 2023 by the authors. Licensee MDPI, Basel, Switzerland. This article is an open access article distributed under the terms and conditions of the Creative Commons Attribution (CC BY) license (https://creativecommons.org/licenses/by/4.0/).

	Parameters	Values
Volume	Layer thickness (mm)	0.03
	Spot Size (mm)	0.15
	Hatch distance (mm)	0.105
	Overlap Factor (mm)	0.7
Contour	Power (W)	192
	Spot size (mm)	0.15
	Beam compensation (mm)	0.075
	Contour Speed (mm/s)	1600
	Hatch Zone Border (mm)	0.065

Table 3 Body process parameters for different specimens (14). R. Sesana, C. Delprete, M. Pizzarelli, M. Crachi, L. Lavagna, D. Borrelli, and A. Caraviello. © 2023 by the authors. Licensee MDPI, Basel, Switzerland. This article is an open access article distributed under the terms and conditions of the Creative Commons Attribution (CC BY) license (https://creativecommons.org/licenses/by/4.0/).

Specimen number	Laser power (W)	Scanning speed (mm/s)	Energy density (J/mm3)
1	192	400	152.38
2	192	600	101.59
3	192	800	76.19
4	230	500	146.03
5	230	600	121.69
6	230	700	104.31
7	230	900	81.13

Powder Range 718, manufactured by Carpenter Additive (Philadelphia, PA, USA), was characterized in detail. Each of the specimens with a 20 mm edge was placed strategically on the fusion platform. The platform had four quadrants, which had seven specimens in each of the quadrants (Ref 14). The laser beam scanning strategy is an island scanning strategy. This strategy divides each layer into smaller islands, scanned in random order, maintaining perpendicular to the scanning vectors of the neighboring islands (Ref 38, 39). While depositing subsequent layers, the islands are shifted in both the x and y directions of the deposition plane (Ref 40).

Inconel^{TM} 718 is a superalloy of nickel, which is weldable and derives its strength through solid solution and precipitation hardening. Depending on the processing and heat treatment, the precipitates enriched with Nb and Mo in a Ni-Cr-based γ matrix form various types of phases, including γ′, γ″, and δ, and

carbides like MC, M6C, and M23C6. The secondary phases are typically formed between 620 and 760 °C when alloying elements such as Al, Ti, and Nb are dissolved in the matrix. The standard thermal treatment (Ref 30) was carried out in an industrial oven that was not pressurized or controlled in atmosphere. The treatment cycle of temperature vs. time is represented in the chart in Fig. 3.

The polishing was carried out through a sander machine (grit sizes 320, 800, 2500) and water coolant. The average surface roughness Ra of the polished specimens is then obtained as 0.06 µm, and the standard deviation is 0.04 µm. This process is used to ensure the hardness analysis is conducted relative to the body material to prevent abnormal behavior because of the contour skin, up-skin, or down-skin, particularly following the non-controlled atmosphere heat treatment. The density of each given specimen is determined using Archimedes' technique (14). The hardness specimen preparation was conducted through the machining removal, in the XY plane tests of the down-skin and the XZ/YZ plane of the contour layer skin (14).

2.3 Hardness Measurement

The hardness was determined by an Innovatest Nemesis 9000 durometer and linked with Impressions tester control and Workflow software. This method is described, and the results are presented in (Ref 14). The collection of data follows standard EN Iso 6507 (Ref 41, 42).

The hardness of Inconel^{TM} 718 printed with LPBF was tested using a DOE method, as shown in (Ref 14). Each sample was tested on perpendicular surfaces, and five repetitions of each measuring configuration were obtained at room temperature. The mean of the five measures on each surface was taken as the hardness value. Evaluation of hardness was done in the deposition base plane (XY plane) and the building job direction (Z). Figure 4 indicates a schematic view of the measured surfaces. Table 4 shows data on the hardness of a chosen subset of specimens in the as-built condition (before heat treatment) and after the heating treatment process. These measurements are made on the YZ /XZ planes and on the XY plane. In each test, the value of hardness is based on the average of five measurements in each surface of XY of each specimen and also the vertical surfaces (XZ/XY planes).

In order to identify the best load, a preliminary experiment was conducted on the basis of various indentation forces by using HV5, HV20, HV50, HV100, and HV120 scales. The depth of indentation and the dispersion of data have shown that HV20 gave the least amount of variance, and a maximum of two melted layers were involved. Hence, the load that was chosen to represent HV20 has been chosen as the reference load to record the hardness results. Vickers hardness tests were therefore conducted at a load of 196 N (20 kgf) and a pyramidal diamond indenter with a dwell time of 10 seconds (Ref 14).

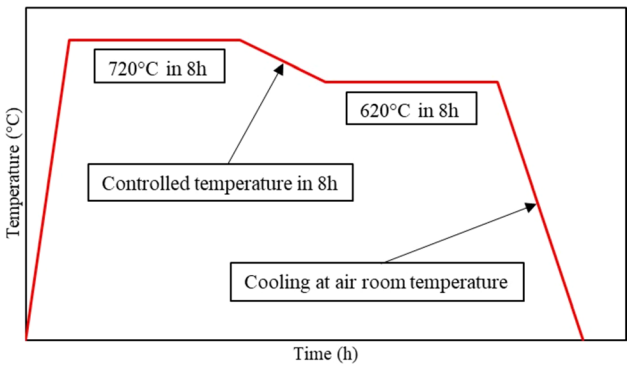

Fig. 3 Temperature-versus-time heat-treatment cycle, followed by air cooling to room temperature

The complete dataset represents that there are 56 observations, including the input and output features determined in the experimental trials. The input data include *P*, *v*, ED, test plane orientation (PO), and sample group. Output data will include the measures of hardness that will be taken right after the printing process (as built) and after heat treatment (heat treatment). The two qualitative sets that constitute the input data cannot be directly handled by any algorithms, but they play a pivotal role in model complexity. Quantitative data are normalized to make coefficients comparable. Therefore, both input categories are trained, resulting in more robust predictive performance.

2.4 Statistical Analysis and ANOVA

Regression and analysis of variance (ANOVA) represent fundamental statistical tools that are largely used in various research areas. They have tangible applications and useful objectives in industrial and commercial projects, particularly in mechanical fields that require improving the efficiency of the targeted output (Ref 43–47).

ANOVA is used to compare the variance contributions of sources and is beneficial to evaluate the effect of the factor that can be controlled on the research findings. The outcome of ANOVA, such as the p value, is the most important result in that it determines whether the independent variables, namely printing parameters and sample orientation, have a significant effect on the measured feature, in the present case heat-treated hardness (Ref 48). The current study includes five different factors (N independent variables); therefore, an N-Way ANOVA was implemented.

2.5 Particle Swarm Optimization and Genetic Algorithm

Genetic algorithm (GA) and particle swarm optimization (PSO) are specific in optimizing parameters of predictive models, and design processes and system performances in areas such as mechanical engineering (Ref 33). PSO is used for solving complex optimization problems in a wide range of practical softwares which is its widespread use in scientific and industrial approaches (Ref 49–51). The particles (solutions) were initialized randomly in the search space, and then while changing each particle's direction (velocity), every particle holds its best value. Then, the best value of all personal best values is taken as the global best value (swarm best value) (Ref 52). GA is a multi-path algorithm that searches many peaks in parallel, hence reducing the possibility of local minimum trapping and solving the multi-objective optimization problems (Ref 53). The GA process emphasizes the interplay between population, selection, crossover, and mutation (Ref 54, 55). This algorithm works iteratively by successively applying these operators in each generation till a termination criterion is satisfied (Ref 56).

Both PSO and the GA seek the correct global optimal solution, but the latter requires spending more time on computations. The PSO is computationally more efficient as compared to GA because it has fewer function calls (Ref 57,

Table 4 Process parameters and measured hardness data of selected specimens (Adapted from Ref 14)

Input parameters					Hardness	
Laser power	Scan speed	ED	Plane	Sample no.	As built	Heat treatment
192	400	152.38	ZX/ZY	D	302	491
230	600	121.69	XY	B	291	474
192	800	76.19	XY	B	284	487
230	700	104.31	XY	D	292	475
230	600	121.69	XY	C	286	474
230	500	146.03	XY	A	284	474
230	700	104.31	XY	A	282	474
230	600	121.69	ZX/ZY	D	383	539
230	500	146.03	ZX/ZY	D	327	481
192	800	76.19	XY	A	287	485
230	700	104.31	ZX/ZY	A	316	478

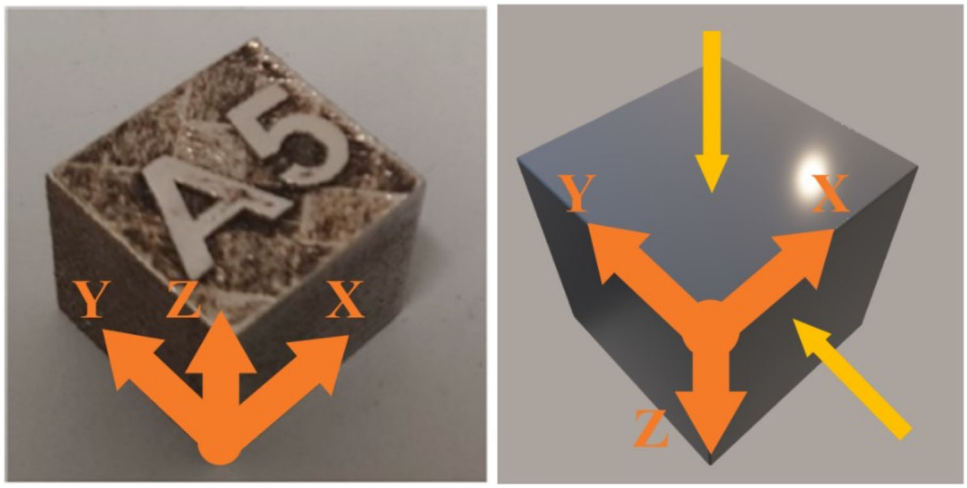

Fig. 4 Surface and local specimen measurement system

58). The advantages and drawbacks of the suggested optimization method were reviewed in (Ref 59, 60). In this section, a nonlinear relationship between parameters was considered. Although there are infinite possibilities of relationships between input and output as expressed by deterministic expressions as an equation, this work will deal with single and two relationships between parameters. Equation 2 is introduced as the resultant formula.

$$\begin{aligned} y =& b_1 x_1^{b_2} + b_3 x_2^{b_4} + b_5 x_3^{b_6} + b_7 x_4^{b_8} + b_9 x_5^{b_{10}} + b_{11}^{x_1} + b_{12}^{x_2} \\ &+ b_{13}^{x_3} + b_{14}^{x_4} + b_{15}^{x_5} + b_{16}\left(\frac{x_1}{x_2}\right)^{b_{17}} + b_{18}\left(\frac{x_2}{x_3}\right)^{b_{19}} + b_{20}\left(\frac{x_3}{x_4}\right)^{b_{21}} \\ &+ b_{22}\left(\frac{x_4}{x_5}\right)^{b_{23}} + b_{24}\left(\frac{x_1}{x_3}\right)^{b_{25}} + b_{26}\left(\frac{x_1}{x_4}\right)^{b_{27}} + b_{28}\left(\frac{x_1}{x_5}\right)^{b_{29}} \\ &+ b_{30}\left(\frac{x_2}{x_4}\right)^{b_{31}} + b_{32}\left(\frac{x_2}{x_5}\right)^{b_{33}} + b_{34}\left(\frac{x_3}{x_5}\right)^{b_{35}} + b_{36} x_1 x_2 \\ &+ b_{37} x_2 x_3 + b_{38} x_3 x_4 + b_{39} x_4 x_5 + b_{40} x_1 x_3 + b_{41} x_1 x_4 \end{aligned} \quad \text{(Eq 2)}$$

In the current formula, b_1 to b_{45} are related to fixed equation coefficient that describes the overall relation between input parameters in 3D printing and the hardness of heat-treated samples as output, and x_1 is related to P, x_2 is related to v, x_3 is related to ED, x_4 is related to PO, and x_5 is related to sample number. In the above formula, all the parameters must be quantitative; therefore, a suitable conversion procedure is required for qualitative parameters like PO and sample number, as described in the results and discussion section.

2.6 Machine Learning

With recent progress, experimental data have started pouring in bulk, with large databases containing critical properties of materials. Such large databases, when judiciously used with the ML solution, hold great promise for improved processes in the manufacturing of materials and overall efficiency (Ref 61).

Support Vector Machines (SVMs) are well-known for their huge impact in addressing a variety of classification issues (Ref 62). The various salient points discussed about SVR are the Epsilon-Insensitive Zone, Function Approximation, Kernel Options, and Algorithm Sequence, all implemented in sequence to arrive at the final regression coefficient to refine the predictive methodology (Ref 63, 64). SVR is an extension of linear regression, which is nonlinear. It uses the functions of the kernel to map the data to a more dimensional feature space, which allows linear separability. The aim is to determine the smoothing function that is allowable in this space to maximize

regression accuracy, according to the following definition in Eq 3.

$$y(x) = f(x) = \sum_{i=1}^{N} (\alpha_i^* - \alpha_i) k(x_i, x) + b \quad \text{(Eq 3)}$$

The variables $\boldsymbol{\alpha_i^*}$ and $\boldsymbol{\alpha_i}$ are Lagrange multipliers. The kernel function is defined by a linear dot product on the nonlinear mapping $\boldsymbol{k(x_i, x)}$. The coefficients $\boldsymbol{\alpha_i^*}$ and $\boldsymbol{\alpha_i}$ in Eq 3 are derived by minimizing the regularized risk functional. It has the following definition in Eq 4.

$$R_{reg}[f] = \frac{1}{2}\|\omega\|^2 + C\sum_{i=1}^{1} L_\varepsilon(y) \quad \text{(Eq 4)}$$

The method also operates with the help of support vectors and enhances the regression performance to minimize errors. It involves other settings, such as C and ω, to seek an acceptable compromise between complexity and the tolerance of error. A constant known as C determines the trade-off, and a value known as ω is an indicator of the complexity of the model. The following definition deals with the ε, sensitive loss function, denoted $L_\varepsilon(y)$, according to Eq 5.

$$L_\varepsilon(y) = \begin{cases} 0, |f(x) - y| - \varepsilon < 0 \\ |f(x) - y| - \varepsilon, |f(x) - y| - \varepsilon \geq 0 \end{cases} \quad \text{(Eq 5)}$$

Gaussian process regression (GPR) is an effective and nonparametric way of approaching regression problems and, as such, can be used in a case where we want to both explore and exploit (Ref 65, 66). GPR in combination with Bayesian optimization and hyperparameter optimization is an opportunity to be able to interpret in probabilistic terms and take the direction of the most effective solution search (Ref 67). GPR offers probabilistic interpretations and directs the search process to the optimal solution when it is used together with Bayesian optimization and hyperparameter tuning. According to the following definition in Eq 6, the GPR-function is the weighted sum of the basic functions (Ref 68).

$$y(x) = f(x) = \sum_{i=1}^{N} w_i \phi_i(x) + \sigma_f \epsilon = W^T \phi(x) + \sigma_f \epsilon \quad \text{(Eq 6)}$$

It is composed of three terms: W is the weight matrix of the output, $\phi(x)$ is the value of the N basis functions at the point x, and ϵ is the white noise model with correlation σ_f across noise models.

In addition, the GPR model, thanks to the flexibility of the kernel functions, allows accommodating a variety of problems and data types (Ref 69). Finally, the likelihood of a certain function ($f(x)$) is provided, and the best weight is achieved by solving it, taking into consideration the noise and uncertainty of the system. This model, unlike the SVR model, has a robust solution.

As the neural network (NN) learns, the weights and the strengths of these connections change. This learning process is referred to as training (Ref 70). The artificial neural network (ANN) is a very useful method of prediction. The ANN model is able to depend on input data to predict future outcomes effectively (Ref 71). The ANN typically includes a single hidden layer and is suited for less complex projects. A deep artificial neural network (deep ANN) is an ANN with multiple hidden layers. In the same, a summary of the advantages and disadvantages of the proposed optimization algorithm is reported (Ref 72–74).

Random tree (RT) is a supervised ML algorithm that is applied in building predictive models, both for classification and regression problems. A random forest algorithm employs a random set of decision trees to calculate the optimal solution. A typical decision tree recursively subdivides the data. The objective at each division, starting from the root node, is to maximize the information gain achieved by that split (Ref 75–77).

2.7 Model Performance

Evaluation or error metrics, also known as performance metrics, are some of the essential operational tools in ML prediction models as well as regression analysis. These metrics are a type of logical and mathematical tool. The aim of these tools is to assess the accuracy of predicted outcomes by comparing them to the actual results (Ref 78). Because each prediction includes some error, these models must be measured to compare the performance of different ones and evaluate (Ref 78, 79).

Root Mean Squared Error (RMSE) or Root Mean Squared Deviation, Eq 7, is a measure of the mean squared error. That is, RMSE is the standard deviation of the errors in the predictions, and it is a measure of how well the line of best fit closely approximates data which are observed data (Ref 80). Mean absolute error (MAE) measures the vertical difference (absolute value) between an actual value and its predicted value. MAE provides a clear explanation of the average error in the same units as the target variable. This makes it easy to understand and communicate (see Eq 8) (Ref 81). Our performance measure of regression models is the Mean Absolute Percentage Error (MAPE), which is an intuitive relative error measure (Eq 9). It is particularly useful in assessing model, the usefulness of which is based on their ability to identify relatively large changes and not necessarily absolute deviations. However, MAPE can only work with positive values and inherently biases low forecasts, so MAPE is less applicable to models where it is expected that large errors are still possible (Ref 82).

The predictive agreement is evaluated by Nash–Sutcliffe efficiency (NSE). The value of NSE is 1 in the event of a perfect model, 0 in the event of a performance equal to the observed mean, and negative in the event of worse predictions than the observed mean. It is given by Eq 10. (Ref 83).

The coefficient of determination, R^2, is more complex when applied to nonlinear regression models or other nonlinear approaches, such as ANN-based predictions. In these cases, R^2 can fall outside the typical 0 to 100% range or even have negative values. Such a negative value indicates a poor fit of the model to the data (Ref 84). The literature discusses eight different formulas for R^2. For nonlinear regression, where the model is not linear, a specific formula, Eq 11, is used to calculate the R^2 (Ref 85–87).

$$\text{RMSE} = \sqrt{\frac{1}{n}\sum_{1}^{n} \left(Y_{\text{pre}} - Y_{\text{act}}\right)^2} \quad \text{(Eq 7)}$$

$$\text{MAE} = \frac{1}{n}\sum_{1}^{n} \left|Y_{\text{pre}} - Y_{\text{act}}\right| \quad \text{(Eq 8)}$$

$$\mathrm{MAPE} = \frac{1}{n}\sum_{1}^{n}\frac{\left|Y_{\mathrm{pre}} - Y_{\mathrm{act}}\right|}{Y_{\mathrm{act}}} \quad \text{(Eq 9)}$$

$$\mathrm{NSE} = 1 - \frac{\sum_1^n \left(Y_{\mathrm{act}} - Y_{\mathrm{pre}}\right)^2}{\sum_1^n \left(Y_{\mathrm{act}} - \overline{Y}_{\mathrm{act}}\right)^2} \quad \text{(Eq 10)}$$

$$R^2 = 1 - \frac{\sum_1^n \left(Y_{\mathrm{act}} - Y_{\mathrm{pre}}\right)^2}{\sum_1^n \left(Y_{\mathrm{pre}} - \overline{Y}_{\mathrm{pre}}\right)^2} \quad \text{(Eq 11)}$$

In the equations above, Y_{act} is the actual value of the output results from the dataset, Y_{pre} is the predicted value from any ML algorithm, $\overline{Y}_{act}$ is the mean value of the actual output, and $\overline{Y}_{pre}$ is the mean value of the predicted output.

The Kling–Gupta efficiency (KGE) is a performance measure that is a composite performance metric suggested by Gupta et al. (Ref 88) to address the shortcomings of the Nash–Sutcliffe efficiency (NSE) by breaking down model performance into correlation, bias, and variability terms. It is given by Eq 12, with its coefficients defined in Eq 13 (Ref 88).

$$\mathrm{KGE} = 1 - \sqrt{(r-1)^2 + (\beta - 1)^2 + (\gamma - 1)^2} \quad \text{(Eq 12)}$$

$$r = \frac{\mathrm{Cov}\left(\mathrm{Y_{act}}, \mathrm{Y_{pre}}\right)}{\sigma Y_{\mathrm{act}} \sigma Y_{\mathrm{pre}}}, \beta = \frac{\mu Y_{\mathrm{pre}}}{\mu Y_{\mathrm{act}}}, \gamma = \frac{\sigma Y_{\mathrm{pre}}/\mu Y_{\mathrm{pre}}}{\sigma Y_{\mathrm{act}}/\mu Y_{\mathrm{act}}} \quad \text{(Eq 13)}$$

In this case, r is the linear correlation coefficient, β is the ratio of bias (mean of predictions to mean of observation), and γ is the ratio of variance in the form of coefficients of variation. The mean and standard deviation are denoted by μ and μ, respectively. Values that are near 1 depict better performance.

The Kruskal–Wallis test is a nonparametric test that was employed to determine the extent to which significant differences in the central tendency among independent groups are significant. In this research, it was used to determine whether the predicted and the observed values of each model belong to the same distribution (Ref 62, 83).

Taylor diagrams are a kind of graphical tool used in many research studies in order to visualize the accuracy of models in targeted studies. This tool is mostly used in the visualization of a system, procedure, or process. The combination of three statistical metrics, including the centered root mean square difference (CRMSD), standard deviations (STD), and the Pearson correlation coefficient, is employed in this instrument. The data measures are put together in a single, easy-to-understand form. The duty of this tool is to enable the evaluation of the specific benefits of various models or the monitoring of changes in a model's performance. The graph shows that using the CRMSD metric, the model overestimates the actual values. The reference point is assigned explicitly on the horizontal axis to be the ground truth. This shows the matching values for the real (Ref 89).

2.8 Structure of Study

The current study consisted of three distinct parts, shown in Fig. 5. The first part (data preprocessing) involved reading data and converting qualitative inputs to quantitative (plane orientation and sample number). After preparing the quantitative data, the statistical analysis and ANOVA are implemented. The second part included model development and optimization algorithms (GA and PSO) to calculate the coefficient of the evaluated formula. Then, the formula by each method was implemented on the input data, and the results were compared with the experimental outputs from the dataset. The last part involved the implementation of five different ML approaches and measuring accuracy metrics for test and training data. However, before implementing ML, a random process divides the dataset into a train and test set. All three parts had performance metrics and accuracy measurements, and the results were compared in order to find the best one for future predictions.

3. Results and Discussion

3.1 Statistical Analysis and ANOVA

The statistical analysis of the data record documented in Table 5 is a structured set of extraction and elaboration of mass data in an effort to unearth some trends and generate useful knowledge. Particularly, the results outlined in Table 2 reveal that the domain range of any parameter should be considered in any further analytical or machine learning activity. This kind of understanding supports the idea that one should remain aware of the distributional nature of variables when developing a model and undertaking tests. The reason is that the formulas and algorithms are valid only in this method within the current data range; however, predictions outside this range may lack accuracy.

Another important insight is the deviation of data, especially the output data. Since they require a greater variation within the output, indicated by a larger STD around the mean value, this makes the lower accuracy and stability, especially with ML algorithms. This means that under such scenarios, optimization would be required. Since this dataset shows a large variety from input to output data, and a large STD, the methodologies in the ML areas should be applied. It is the only reason that data normalization and optimization should be used during the ML process.

To explain the effects of various experimental conditions on the overall outcome of hardness, an ANOVA analysis (nonlinear regression) was performed. To enable rigorous statistical analysis and machine-learning implementation, qualitative factors (plane orientation and sample identifier) were converted to numeric codes and included in the working dataset (see Table 5). Most ML algorithms and many statistical procedures require numeric inputs; encoding categorical variables makes them compatible with regression, tree, and kernel-based methods and permits standard preprocessing steps such as scaling, normalization, and feature selection (Ref 68, 90–93). Encoding also facilitates reproducible cross-validation, automated hyperparameter tuning, and the computation of quantitative importance measures. Care was taken to preserve the categorical nature of each variable: plane orientation was mapped to 1 (XY) and 2 (ZX/ZY), and sample labels A-D were mapped to 1-4; potential risks of introducing spurious ordinality are mitigated by treating these encoded variables appropriately in model selection (for example, using one-hot encoding or categorical-aware algorithms where needed) and by reporting model sensitivity to encoding choices. The converted dataset in Table 5 therefore serves as the consistent, machine–readable input for all subsequent analyses.

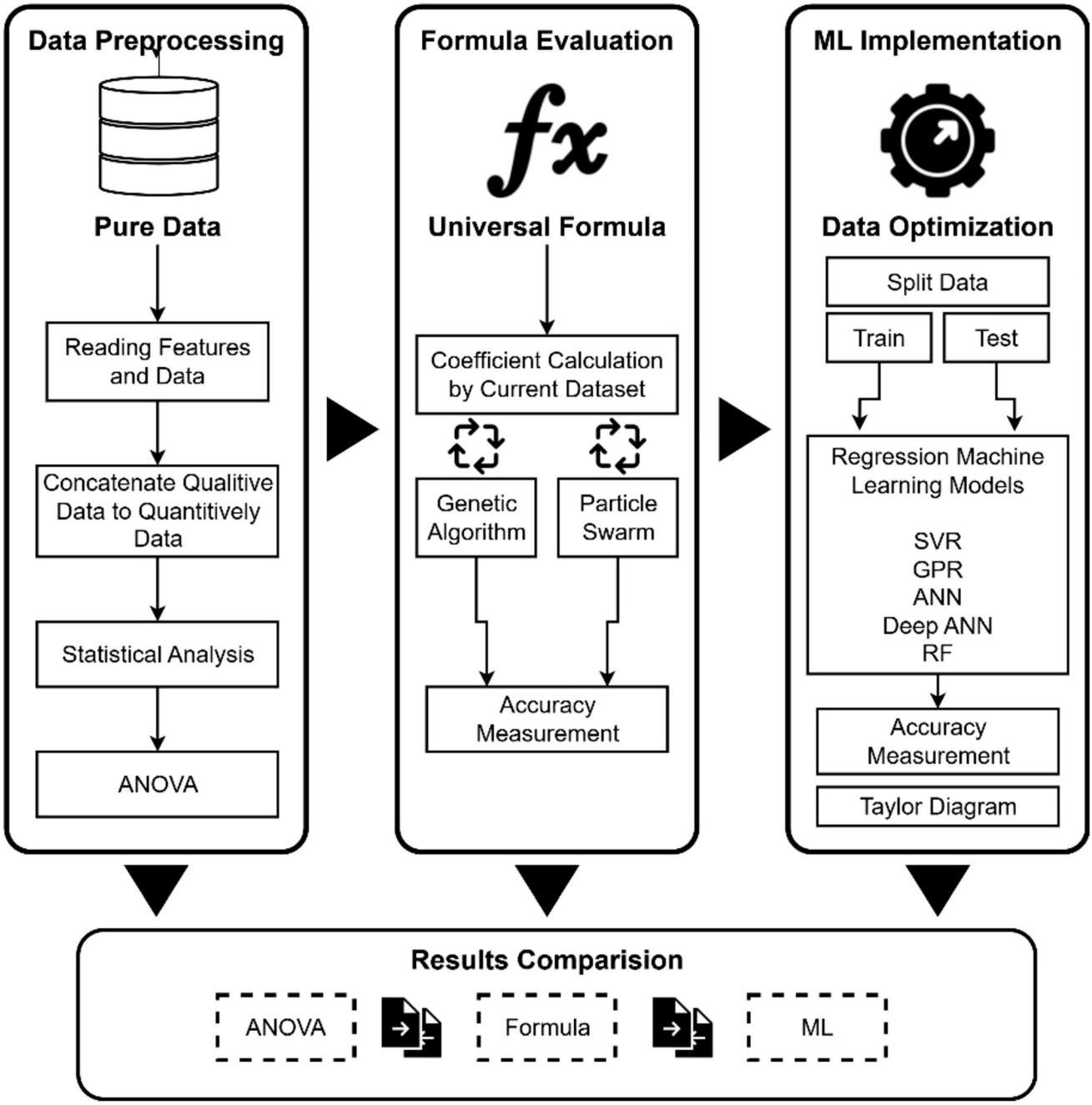

Fig. 5 The study procedure schema

Table 5 Statistical analysis of current 56 data in-out dataset

		Min	Max	Average	STD
Inputs	Laser power	192	230	213.71	18.98
	Scan speed	400	900	642.85	160.52
	Energy density	76.19	152.38	111.90	27.73
	Plane		Qualitative data		
	Sample no.		Qualitative data		
Output	Heat treated	466	541	488.63	22.38

Table 6 ANOVA analysis results

Parameter	Sum Sq.	d.f.	Mean Sq.	F	*p*-Value
Laser power	443.6	1	443.62	1.38	0.2456
Scan speed	4066.4	5	413.28	1.29	0.2852
Energy Density	0	0	0	0	NaN
Plane	9490	1	9490.02	29.61	0
Sample no	1113.5	3	317.16	1.16	0.3362
Error	14421.6	45	320.48		
Total	27535.1	55			

The final results of the heat-treated hardness tests and the corresponding ANOVA are presented in Table 6. It is important to say that the primary output considered in all implementations is the heat-treated hardness. The heating process is carried out by implementing precise monitoring of heat treatment parameters, and the AM part properties can be made into optimized settings to suit the needs of its target application (Ref 94, 95).

The ANOVA test conducted on the current data proved to be of no use in this research as far as the p values of the test are concerned. When the p value is less than 5% (which is equal to 0.05), it is easy to say that this type of variable dependency between input and output is rather considerable. The results, however, indicated that except for PO, all the parameters had a p value over 5%. These results show that key parameters like LP, SS, or ED do not significantly affect the final hardness, which contradicts several prior investigations (Ref 96–98). So, the ANOVA test is unable to show the interdependence of all variables and needs deeper analysis. Complex techniques, including sophisticated mathematics and ML techniques, may be used in future research. Experimental techniques demonstrate that hardness is sensitive to the parameters confirmed by ANOVA; however, it fails to find a comprehensive link to the impact of all parameters on the final outcomes. Consequently, in this study, all parameters were selected for further investigation.

3.2 Formula Evaluation

Current research optimized the relationship between process parameters for Formula 1 and the final heat-treated hardness of products. In this section, a new formula that incorporates five different input variables was developed, shown in Eq 1. It includes five inputs: x_1, x_2, x_3, x_4, and x_5. The formula implementation concentrated on combinations of single and double inputs, yielding 45 coefficients. Although more complex combinations can be taken into account, this combination was enough. An optimization procedure using PSO and GA was used to estimate the coefficients, and this meant that the model captured the underlying relationships effectively.

PSO is intended to solve the optimization task by exploiting the objective function to specify the formula coefficients. MATLAB® software was used in this case. Equation 14 defines the objective function as the sum of squared errors between the predicted and actual values of hardness as drawn from the data. This is called an objective function, where the goal of the optimization process is to make it as small as possible to get the optimal coefficients.

$$\text{objectivefunction} = \sum_{\text{allDataSet}} (y_{\text{formula}} - y_{\text{real}})^2 \qquad \text{(Eq 14)}$$

The algorithm iteration repeats the update steps until convergence criteria are met (a maximum number of iterations, which is defined as 100, or a satisfactory error threshold, which is defined as $1e^{-6}$). The hyperparameters of the current PSO implementation are tabulated in Table 7. The result of 10 iterations using MATLAB® has been obtained with the final formula being presented below in Eq 15 (the coefficients equal to zero have been dropped, and the formula has been simplified to make it easier to read).

$$\begin{aligned} y =& 10x_2^{0.220} + 10x_3^{0.335} + 10x_5^{1.209} + 0.996^{x_1} + 0.761^{x_2} \\ &+ 0.997^{x_3} + 6.463^{x_4} + 6.225^{x_5} + 10\left(\frac{x_2}{x_3}\right)^{0.166} \\ &+ 10\left(\frac{x_3}{x_4}\right)^{0.358} + 10\left(\frac{x_1}{x_4}\right)^{0.074} + 10\left(\frac{x_2}{x_4}\right)^{0.389} \\ &+ 10\left(\frac{x_2}{x_5}\right)^{0.124} + 10\left(\frac{x_3}{x_5}\right)^{0.457} + 50 \end{aligned} \qquad \text{(Eq 15)}$$

This section addresses the optimization problem by minimizing the objective function by means of GAs to find the coefficients of the formula. The objective function computes the sum of squared errors between the predicted hardness (based on the computed coefficients) and the actual hardness values in the dataset, as specified by Eq 15. The update process was further carried out until convergence requirements were achieved either through 100 iterations or the error reduction reaching below 1e−6. The hyperparameters of the presented GA implementation are given in Table 7. The last formula is given in Eq 16 and was determined after ten independent tests in MATLAB®. It is assumed that coefficients that have a zero value have been excluded and that, to make it easier to understand, the formula was simplified (Table 8).

$$\begin{aligned} y =& 0.5x_1^{0.238} + 0.826x_2^{0.604} + 0.125x_3^{0.577} + 4.209x_4^{0.004} \\ &+ 4.815x_5^{0.531} + 0121^{x_1} + 0.999^{x_2} + 0.773^{x_3} + 0.843^{x_4} \\ &+ 0.825^{x_5} + 0.421\left(\frac{x_1}{x_2}\right)^{9.079} + 1.075\left(\frac{x_2}{x_3}\right)^{1.730} \\ &+ 3.423\left(\frac{x_4}{x_5}\right)^{0.039} + 1.423\left(\frac{x_1}{x_3}\right)^{0.296} + 5.176\left(\frac{x_1}{x_4}\right)^{0.051} \\ &+ 0.168\left(\frac{x_1}{x_5}\right)^{1.030} + 0.003\left(\frac{x_2}{x_4}\right)^{1.325} + 0.822\left(\frac{x_2}{x_5}\right)^{0.516} \\ &+ 0.930\left(\frac{x_3}{x_5}\right)^{0.967} + 0.031x_3x_4 + 0.004x_4x_5 + 0.006x_1x_3 \\ &+ 0.004x_1x_4 + 0.131x_1x_5 + 0.056x_2x_4 + 0.074x_3x_5 \end{aligned} \qquad \text{(Eq 16)}$$

The overall results from the PSO and GA optimization methods implemented on input data and formula output are compared one by one with real values, and the accuracy metrics

Table 7 The hyperparameters of the current particle swarm implementation

Hyper parameter	Value / Range	Description
Swarm size	100	The number of particles in the swarm.
Number of iterations	100	The maximum number of iterations or generations the algorithm will run
Inertia weight (w)	[0.1, 1.1]	Controls the influence of the previous velocity on the current velocity
Cognitive coefficient (c1)	1.5	The weight of the particle's own best position (personal best)
Social coefficient (c2)	1.5	The weight of the global best position found by the swarm
Position bounds	[0, 10]	The upper and lower bounds for the particle positions
Convergence criteria*	1e−6 / 1000	Conditions under which the algorithm will stop, such as a maximum number of iterations or a satisfactory error threshold
Random numbers (r1 and r2) [1]	[0, 1]	Random numbers between 0 and 1 used in the velocity update equation

*Parameters that are automatically configured within the particle swarm algorithm

Table 8 The hyperparameters of the current GA implementation

Hyper parameter	Value / Range	Description
Population size	100	Determines the number of individuals in each generation. A larger population size can provide a more diverse set of solutions but may increase computational cost
Number of generations	1000	Specifies how many iterations the algorithm will run. More generations can lead to better solutions but also require more computation time
Crossover probability	0.8	The probability that two individuals will exchange parts of their chromosomes. This helps in combining good traits from different individuals
Mutation function	@mutationpower	Specifies how mutations are applied to individuals
Selection function	@selectiontournament	Determines how individuals are selected for reproduction
Elite count	10	The number of top individuals that are guaranteed to survive to the next generation. This helps in preserving the best solutions found so far

Table 9 Accuracy metrics for evaluated form formula implemented by PSO and GA

Accuracy metrics	Particle swarm	Genetic algorithm
Accuracy (Max)	100%	100%
Accuracy (Min)	92%	82%
Accuracy (Mean)	97%	93%
MSE	349.2	1806.2
RMSE	18.7	42.5
MAE	15.3	35.4
MAPE	3.1%	7.2%
R^2	0.29	−2.7

are implemented on each series of data (Real Value and Formula Value). The overall results are tabulated in Table 9. As shown in Table 9, the PSO provided a better solution due to the lower MSE and MAE, and also the mean accuracy for all the given 56 data points is around 97% with respect to 93% for GA. Furthermore, the generated formula by PSO is also simpler than GA, which aligns with the advantages of PSO with respect to GA mentioned in Table 9.

However, for both solutions, the final result is a single fixed formula that is sensitive to the input domain. Both obtained formulas (Eqs 15 and 16) have the following constraints:

- x_1 the laser power should be in the range of 192-230
- x_2 the scan speed should be in the range of 400-900
- x_3 the energy density should be in the range of 76.19-152.38
- x_4 the plane orientation should be selected from an integer number between 1 and 2
- x_5 the sample number should be selected from an integer number between 1 and 4

These limitations restrict the use case of this formula when used universally, as it only holds true in the existing data. Also, the implementation cannot adapt to any other data domains, and it lacks scalability. In case the set of data is changed or more parameters are introduced, the formula would not be useful anymore with the new observations. Therefore, enhancing new methods to solve these limitations to obtain flexibility and scalability is necessary.

3.3 Machine Learning Implementation

To apply the five different ML algorithms, the dataset was divided into two groups. The dataset was split into 80% training (45 samples) and 20% testing/validation (11 samples) to apply the five ML algorithms. The training subset (45 samples) was used for model fitting, hyperparameter tuning, and cross–validation; the testing subset (11 samples) was reserved for final validation and performance reporting. The property of each group (train and test) is mentioned in Table 10. The train and test datasets exhibited distinct statistical actuality to confirm the efficacy of the data splitting technique and to guarantee an acceptable distribution of the data, but as mentioned before,

Table 10 Statistical parameters of train and test dataset

	Minimum		Maximum		Average		Coefficient of Kurtosis		Coefficient of Skewness		Coefficient of variation	
Variables	**Train**	**Test**	**Train**	**Test**	**Train**	**Test**	**Train**	**Test**	**Train**	**Test**	**Train**	**Test**
Laser power	192	192	230	230	213.10	291.60	1.05	2.04	−0.22	−1.02	8.96	8.69
Scan speed	400	400	900	800	653.30	627.30	1.92	2.13	0.10	−0.23	25.19	26.24
Energy density	76.19	76.19	152.38	152.38	109.90	115.90	1.73	2.01	0.36	−0.15	25.13	23.82
Plane	1	1	2	2	1.60	1.40	1.05	1.32	−0.22	0.57	32.30	36.85
SAMPLE no.	1	1	4	4	2.50	2.50	1.71	1.28	0.03	0.10	44.58	44.80
Heat treated	466	474	541	539	489.70	484.70	2.74	7.40	1.16	2.36	4.73	4.78

Table 11 The all-hyper-parameters used in the implementation

ML models	Hyperparameters	Search space	Selected value
SVR	C	(0.1, 1000)	13.89
	Epsilon	(0.01, 10)	1.39
	Kernel function	polynomial, gaussian, linear	Polynomial degree 3
GPR	Sigma	(0.01, 10)	4.5
	Kernel Parameter	(0.01, 10)	6.5
	Kernel function	RQ, SE, M52, Exp.	RQ
ANN	Neurons in each layer	(5, 20)	5
	Learning rate	(0.01, 1)	0.1
	Activation Function	Relu, Sigmoid, Tanh	Relu
Deep ANN	Hidden layers	(2, 10)	3
	Neurons in each layer	(5, 20)	[8]
	Learning rate	(0.01, 1)	0.1
	Activation Function	Relu, Sigmoid, Tanh	Relu
RT	Minimum Leaf Size	(1, 20)	5
	Maximum Number of Splits	(10, 100)	50
	Split Criterion	MSE	MSE
	Surrogate Decision Splits	(on, off)	on

both of them have the same domain, which is crucial in the realm of ML.

In the process of analyzing, there are hyperparameters that are considered for ML algorithms. The ML models will operate well if their hyperparameters are chosen accurately and properly. In this study, the Bayesian optimization method was employed in order to find the best hyperparameters. MATLAB® software with its standard rules was employed to operate the process of optimizing the variables. The final results are presented in Table 11.

As mentioned above, Bayesian optimization was employed to find the ideal hyperparameters. Speaking of the standard Bayesian optimization, with fivefold cross-validation, was used in the process. Because every model had many hyperparameters, in this study, several important hyperparameters were considered, and the remaining were set to default values in the software package. Three parameters, such as the regularization parameter (C), epsilon, and the type of kernel function, were optimized for using the SVR model. The C parameter is used for the level of penalty applied to data points that are outside the particular region. The epsilon parameter gives a range of tolerance of the error of the regression line, outside which the deviations need not be deemed as errors. The flexibility of the fitting function is controlled by the type of kernel function. For the GPR model, the sigma parameter of the squared exponential kernel and the type of kernel covariance function were optimized. The kernel covariance function could be chosen from a variety of options: rational quadratic, squared exponential, Matern kernel with parameter 5/2, and exponential. These options defined the flexibility of the model to better fit the input data. For the ANN and deep ANN models, the number of hidden layers, the total number of neurons in each hidden layer, the activation function, and the learning rate were optimized. The difference between standard and deep neural networks is the size of the hidden layer, where for the standard one, just one hidden layer is considered, while for the deep model, more than two hidden layers are considered. The number of neurons in each layer seemed to improve the performance of the ANN model, but it also increased the risk of overfitting. An activation function is crucial for determining how the network processes and outputs data. There are several choices for activation functions like sigmoid, ReLU, and tanh, but the ReLU activation function is a linear function that is suitable for linear and nonlinear problems. For RT, the smaller leaf sizes can capture more detail but may lead to overfitting. A maximum number of splits will control the maximum number of decision splits in the tree. Greater splits may make any given model more complex. To address the issue of missing data, one takes advantage of missing data through the use of Surrogate Decision Splits, which seek alternative splits. Pruning involves removing branches that have little importance to reduce overfitting.

After performing up to 100 iterations for the final selection of each hyperparameter and comparing the accuracy metrics values as the verification factors, every algorithm was trained on 45 data points. As shown in Table 12, ML implementation does not provide acceptable results for finding the best solution, and therefore final data distribution around the perfect prediction line is not sufficient. Although MAPE was so low, under 6% for all five methods, MAE for all five methods is around

Table 12 Accuracy metrics for training process non-optimized parameters

Data set	Accuracy metrics	SVR	GPR	ANN	Deep ANN	RT
Train	RMSE	29.8	22.0	21.5	40.7	22.8
	MAE	21.7	17.5	16.8	29.5	16.7
	MAPE	4.3	3.5	3.4	5.9	3.3
	KGE	−0.54	0.10	0.23	−2.11	0.12
	NSE	−0.62	0.07	0.13	−2.18	0.3
	R^2	−0.68	0.08	0.12	−2.20	0.01

Table 13 Accuracy metrics for training process optimized parameters

Data set	Accuracy metrics	SVR	GPR	ANN	Deep ANN	RT
Train	RMSE	62.5	20.4	28.2	38.8	75.3
	MAE	47.8	16.4	21.9	31.5	62.4
	MAPE	4.7	1.5	2.1	3.1	6.5
	KGE	0.79	0.99	0.99	0.97	0.95
	NSE	0.90	0.99	0.98	0.96	0.89
	R^2	0.91	0.99	0.98	0.96	0.88

20%. NSE and KGE are not acceptable. Additionally, because of the large amount of data deviation, which is shown in the R^2 parameter, these six implementations are not acceptable for any future metric implementation. Therefore, these methods are not stable in the training process. The optimization process happened at two distinct levels, the first one happens at the hyperparameters side, which is implemented and reaches acceptable accuracy, but not sufficient for method stability, so the other side is at the data preparation to reach a better solution.

An essential process of an ML is feature engineering, accepting a feature vector as an input, and delivering a prediction. These are supervised trained models, and in these models, the feature vectors that are presented correspond to the actual expected output. Some features may be improved through approaches like normalization, logarithmic conversion, and formalization of new features with polynomials that make the data more suitable for being worked by linear models. Moreover, developing additional characteristics, such as interaction terms, and identifying the most relevant ones via various approaches may substantially improve model performance and stability (Ref 99, 100).

Several methods are proposed for feature engineering in the section on feature construction, combining input and output data with specific formulas to capture their interaction effects that enhance the stability of ML implementation. In the following section, to reach a better solution and a stable ML algorithm, the new output is based on the combination of inputs and outputs proposed by Eq 17. Although this equation is based on the fixed input data, and therefore the final results can be easily converted to the main hardness value, the flow is able to rollback, which is important to reach a final reasonable solution.

$$\text{Hardness}_{\text{optimized}} = \text{Hardness}_{\text{HT}} + \text{LP} + \left(6.43 - \frac{\text{SS}}{100}\right) - \text{ED} + 20^{\text{Plane}} + 100 * \text{Sample Number} \quad \text{(Eq 17)}$$

The optimized training results based on the two mentioned optimized approaches (hyperparameter optimization and feature engineering based on Eq 17) are illustrated in Fig. 6(a), (b), (c), (d), and (e). These figures show the correlation between predicted results during the process and real hardness from the perfect prediction line. The accuracy metrics for the training process optimized parameters are tabulated in Table 13. As results illustrate, the GPR and single-layer ANN proposed the best training results. The R^2 for both methods is more than 0.98 (0.99 for GPR and 0.98 for ANN), which is perfect in the ML domain. The formula changes the domain of data, and now the new output data have the minimum and maximum values of 639.34 and 1448.53, respectively with a mean value of 1070.3 which affects the other accuracy metrics parameters, and it is impossible to compare RMSE before and after feature engineering, but the MAPE parameter indicates a mean absolute error in percentage and also it is comparable. The MAPE did not change reasonably and remained under 3.5% and 3.4% for GPR and ANN, respectively. This indicates that both optimization approaches provided the best solution by these methods. The results of KGE and NSE show that GPR and ANN are the best models for training. This means that they achieve agreement with observations in terms of correlation, bias, and variability. High NSE shows accurate and calibrated training performance.

The SVR method reaches a good R^2 and is more than 0.91. Furthermore, the absolute mean percentage error increases from 4.3% to 4.7%, but the total mean accuracy remains around 95%, which is also acceptable in the engineering domain.

Although the deep ANN provided complex solutions in some areas, it did not do so in others. Like the other method, the optimization process improved the deep ANN, and R^2 reached the perfect result of 0.96. Furthermore, the MAPE decreased from 5.9% to 3%. The last method, RT, also just reached an R^2 of about 0.88 and a MAPE under 7%.

The overall results from the current section show that all the methods, except RT, with the lowest R^2 among all models, have sufficient stability and accuracy (more than 90%), and for continuing investigation and implementation on testing data is suitable; however testing data should also be optimized output like a training dataset for implementing the testing procedure.

After training data, each method reached stable and reasonable parameters within its algorithm. It is time to test

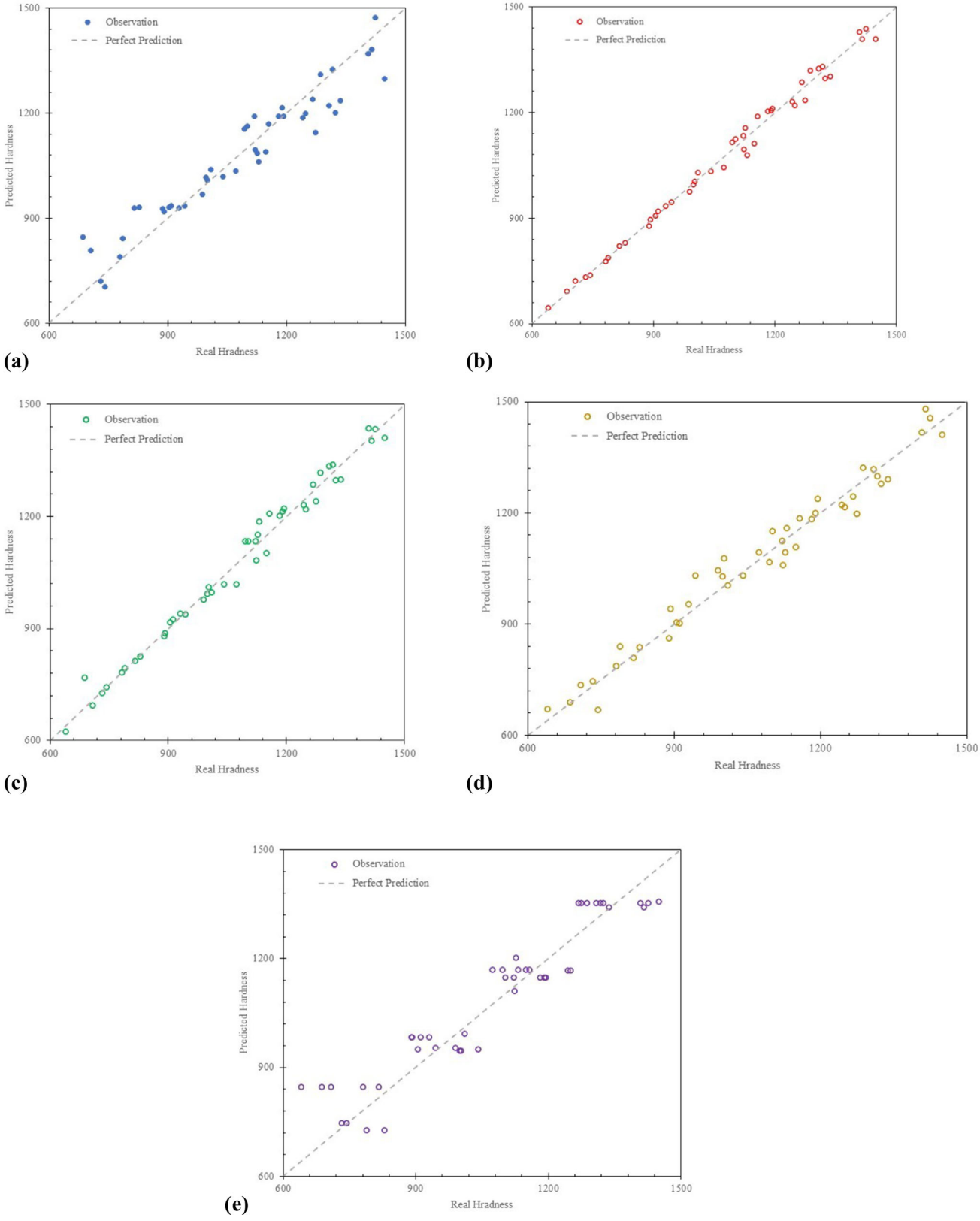

Fig. 6 Optimized training results (a) SVR, (b) GPR, (c) ANN, (d) Deep ANN, (e) RT

Table 14 Accuracy metrics for testing process optimized parameters

Data set	Accuracy metrics	SVR	GPR	ANN	Deep ANN	RT
Test	RMSE	36.5	17.7	16.1	22.0	56.7
	MAE	26.1	13.6	13.3	15.4	44.2
	MAPE	2.6	1.3	1.3	1.4	4.6
	KGE	0.92	0.99	0.98	0.97	0.89
	NSE	0.97	0.98	0.99	0.99	0.96
	R^2	0.98	0.99	0.99	0.99	0.95

the models on test data. Test data are a small portion of the main dataset, which is completely split from the training dataset and includes data within the domain of the training dataset. Therefore, the final results of testing these 13 sets of data are illustrated in Fig. 7(a), (b), (c), (d), and (e), for SVR, GPR, single-layer ANN, deep ANN, and RT, respectively. Furthermore, the accuracy metrics which are associated with the final testing results are tabulated in Table 14.

As a result of the training process, the GPR and ANNs bring sophisticated results with respect to the other methods. Again, in the testing procedure, both of them had a perfect R^2, which is 0.99, and the lowest MAPE (1.3 for both GPR and ANNs). The KGE and NSE results also follow and confirm that these ML methods capture the behavior with minimal bias. These methods indicate stable sets and calibrated fits on the test outputs.

So these methods were selected among them as the best ML implementations.

At the next level, the SVR and deep ANN with R^2 of more than 0.98 and MAPE of less than 2.6% provided acceptable results, but again RT method has the lowest R^2 of about 0.95 and the highest MAPE of about 4.6% in training results. Furthermore, the results of KGE and NSE for SVR and RT methods are less than other accurate ML methods mentioned above. Overall, these methods provided the worst results among the mentioned ML algorithms (Table 13).

The process of optimization is based on feature engineering, and the output data are changed to a new version which are calculated by Eq 18, but the final output which is measured by the testing process should be calculated by the rollback process, the rollback process means calculated the final predicted hardness from newly generated parameter in the testing process by Eq 17 which is reversed version of Eq 18.

$$\text{Hardness}_{\text{Predicted}} = \text{Hardness}_{\text{optimized Test}} - \left(LP + \left(6.43 - \frac{\text{SS}}{100}\right) - \text{ED} + 20^{\text{Plane}} + 100 * \text{Sample Number}\right) \quad \text{(Eq 18)}$$

In the following formula, $\text{Hardness}_{\text{optimized Test}}$ is generated from the testing process and then put in Eq 18 with related input including LP, SS, ED, PO, and sample number, and because these input parameters for each set of data are fixed, the rollback process acts like a linear formula. This step converts the optimized output back to the original hardness scale for a fair comparison. The $\text{Hardness}_{\text{Predicted}}$ generated from this method is optimized predicted hardness which is compared with both real hardness and non-optimized predicted hardness for all five methods; the overall results are mentioned in Fig. 8(a), (b), (c), (d), and (e) and also Table 14. The testing stage is itself a prediction on unseen data used for evaluation, and in the same Eq. 18, rollback step was applied in practical prediction for new inputs.

As mentioned before, the SVR method did not bring the best results in both the training and testing processes related to MAPE and R^2; however, the accuracy remains acceptable at more than 95%. Based on the results in Table 14 for RT, the mean accuracy for both optimized rollback and non-optimized models is still high.

On the other hand, the GPR method brings the best results for the training and testing process, and is one of the selection candidates for the proposed study. In Table 14 for GPR and Fig. 8(b), the overall results of GPR rollback are also acceptable and bring the absolute mean percentage error around 2.8% and mean accuracy around 97%, which is similar to 98% accuracy of the non-optimized process, and less than 1% change in accuracy is absolutely negligible in the field of mechanical engineering.

Like GPR, the single-layer ANN with 5 hidden layers and ReLU activation function also brings the best results for both the training and testing processes. The comparison between a non-optimized ANN, which is mentioned in the column of ANN in Table 14, and the optimized rollback shows that both have the same mean absolute error (2.5% for non-optimized and 2.7 for optimized rollback), and it is clear that both methods don't have any difference, and the optimized process acts perfectly on model stability. Therefore, this ANN method was selected as the best implementation in the current study.

In this study, the deep ANN implementation did not bring the best results and was chosen after the ANN and GPR methods at the third stage. However, by comparing the final hardness results from the prediction method both in the non-optimized process and optimized rollback process, which is mentioned in Table 14 for deep ANN, the accuracy remains acceptable and is more than 97%, and the mean absolute error is not more than around 3%, and also the accuracy difference between optimized and non-optimized is around 1%, which is reasonably acceptable.

The last implemented method is RT, which has the worst results among these five ML methods, both in the training and testing processes, in an optimized manner. From Table 14 for RT, the optimized rollback also brings the mean absolute percentage error around 9%, which is increased by 7% compared to the mean absolute percentage error by the non-optimized process, and is absolutely not acceptable in the current study.

Kruskal–Wallis was used to test the hypothesis that the central tendency of the predicted and observed values is identical, as shown in Table 15. The significance of this nonparametric method is that the method evaluates the statistical consistency of model results, not on the assumption of a normal distribution. H_o implies that the central tendency between predictions and observations does not differ significantly. H_o is not rejected when p is less than 0.05, and H_o is rejected when p is greater than or equal to 0.05, which implies a significant difference (Ref 83). The findings indicated that GPR, ANN, and deep ANN had a strong correlation between predicted and observed means, which proved their reliability and stability throughout the training.

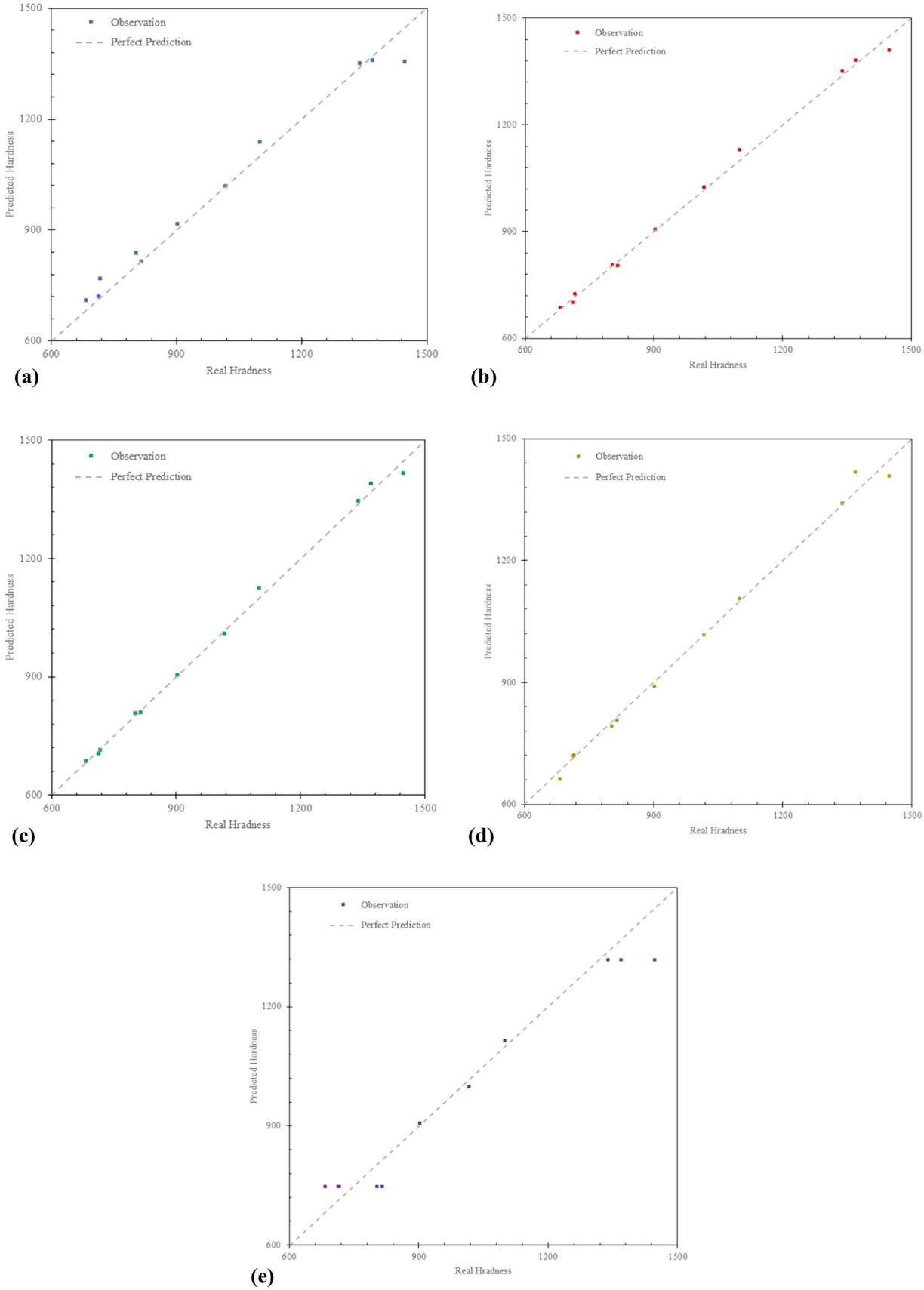

Fig. 7 Optimized testing results (a) SVR, (b) GPR, (c) ANN, (d) Deep ANN, (e) RT

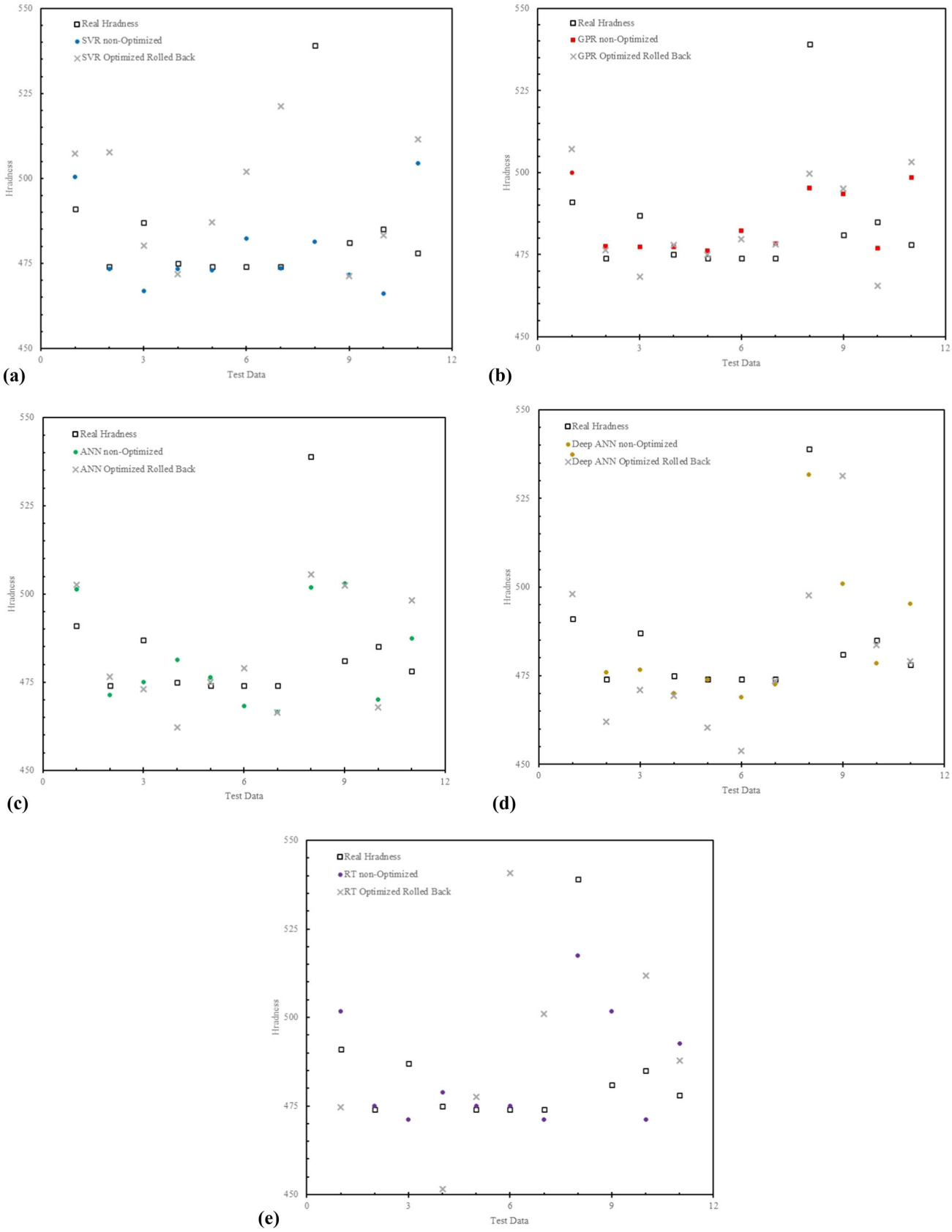

Fig. 8 Comparing experimental hardness with non-optimized and optimized rollback by (a) SVR, (b) GPR, (c) ANN, (d) Deep ANN, (e) RT methods

Table 15 Results of hardness with non-optimized and optimized rollback

HT	SVR	SVR roll back	GPR	GPR roll back	ANN	ANN roll back	Deep ANN	Deep roll back	RT	RT roll back
491	500.4	507.2	500.1	507.2	501.3	502.7	537.4	498.1	501.7	474.6
474	473.4	507.8	477.5	476.4	471.3	476.4	476.0	462.0	475.0	417.3
487	466.9	480.2	477.3	468.2	475.1	473.1	476.7	471.1	471.2	411.8
475	473.5	471.9	477.3	478.0	481.4	462.2	470.0	469.4	478.8	451.6
474	473.0	487.1	476.3	475.0	476.3	475.0	473.9	460.4	475.0	477.6
474	482.3	502.0	482.3	479.8	468.2	478.9	469.0	453.9	475.0	540.7
474	473.5	521.3	478.4	478.2	466.6	466.4	472.6	473.6	471.2	501.0
539	481.3	445.4	495.4	499.7	502.0	505.5	531.7	497.6	517.4	407.9
481	471.6	471.3	493.6	495.1	503.0	502.4	501.1	531.4	501.7	431.3
485	466.2	483.3	476.9	465.5	470.2	467.9	478.6	483.6	471.2	511.8
478	504.5	511.5	498.5	503.3	487.3	498.3	495.4	479.1	492.5	487.8
Mean Accuracy	97%	95%	98%	97%	98%	97%	98%	97%	98%	91%
MAE	14.0	26.1	11.3	13.6	12.2	13.3	11.0	15.4	9.7	44.2
MAPE	2.8	5.3	2.3	2.8	2.5	2.7	2.3	3.1	2.0	8.9

Table 16 Kruskal–Wallis test *p*-values at the 95% confidence level

Model	*p*-value	H_o
SVR	0.06	Reject
GPR	0.00003	Accept
ANN	0.01	Accpet
Deep ANN	0	Accept
RT	0.01	Reject

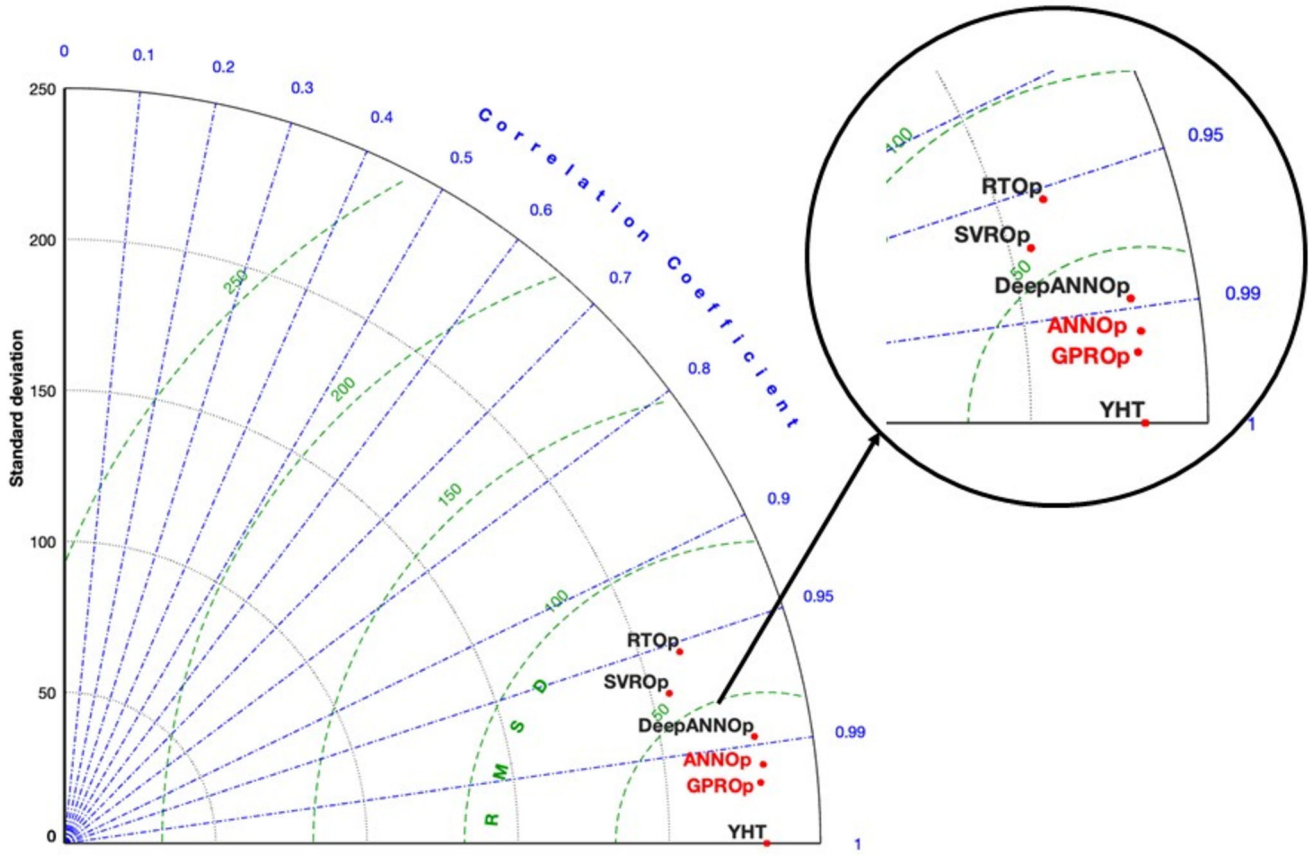

Fig. 9 Taylor diagram for all optimized ML methods

They pass this test, so these models are well calibrated and they reflect the underlying pattern of the data with only a small systematic bias. Conversely, neither SVR nor RT satisfied this criterion, with a bigger deviation between their forecasted values and real values. This is due to the results of the training and the test accuracy metrics. It implies that they are ineffective in

extrapolating the underlying associations in the dataset and are more likely to give biased or volatile results than GPR and ANN.

3.4 Taylor Diagrams

The STD, Pearson correlation, and centered RMSD are the three important metrics that are used in the Taylor diagram, which is used to compare the performance of different ML models. These metrics determine and show the degree of similarity between the predictions generated by ML models and the outcomes of experiments. In cases where one ML model performs successfully, this will be due to a low RMSD, following a high correlation. Also, its standard deviation closely matches the experimental outcomes. Therefore, the targeted model will be positioned closer to the experimental point on the graph. This would ensure its higher accuracy in comparison with other models. From the Taylor diagram (Fig. 9), the GPR and ANN methods provided the best solution, and again, this method was suggested as the best method during the entire process (Table 16).

4. Conclusions

This paper focuses on the evaluation of the impact of the printer setting parameters on the heat treatment of the hardness of the LPBF technique on the M2 Series 5 3D printer model by General Electric Additive Solutions with Inconel^{TM} 718 as a material. Laser power, scan speed, energy density, orientation of test plane, and sample group were used as the prime input parameters. The hardness measurements were obtained both before and after the heat treatment in two planes and on 28 particles.

A sophisticated formula was developed based on input and output data. These data are single and sequential relations among five parameters, having 35 different coefficients. This formula was solved through two optimization techniques, namely PSO and GA. Although the results obtained possessed low mean absolute percentage errors (3.1% for PSO and 7.2% for GA), the data deviation was too great, and the values of R^2 were under 0.3. So, this indicates poor applicability for general use and inflexibility with new data or parameters.

In order to overcome these drawbacks, ML techniques were taken into account. They included five regression algorithms: SVM, GPR, single-layer ANN, deep ANN, and RT. First of all, the data were divided into 45 training data points and 11 testing data points. Optimization of the hyperparameters was done using the Bayesian algorithm, but the R^2 values were low or negative, indicating that it was not stable.

The best results were observed in GPR and both ANN methods, as they had the highest values of R^2, NSE, and KGE, ranging between 0.97 and 0.99, and the lowest values of MAPE, MAE, and RMSE on the test data, thereby showing them as the best solutions. There was a novel method, rollback process, that optimized the predicted hardness against the actual hardness. To analyze the effectiveness of models and prove the validity of these ML techniques, the Kruskal–Wallis test and Taylor diagram were also employed.

The predictive results are constrained by the limited dataset size ($n = 56$), which reduces statistical diversity, increases sensitivity to measurement noise, and raises the risk of overfitting despite the safeguards applied (train–test separation, cross-validation, regularization, and multiple performance metrics: R^2, NSE, KGE, MAPE). Consequently, model performance and uncertainty estimates are most reliable within the sampled domain, and we explicitly note that expanding the experimental dataset would improve robustness, reduce variance in model estimates, and extend extrapolation capability.

The models and empirical formulae are interpolative and valid only inside the experimental parameter window (laser power 192-230 W; scan speed 400-900 mm/s; energy density 76-152 J/mm3; two build orientations; four sample groups). Predictions outside these ranges may be physically inconsistent because the models are data-driven and not constrained by first-principles thermal models. Likewise, the trained models are material-specific to LPBF Inconel™ 718—driven by Ni-based solidification and precipitation hardening—and are not directly transferable to other alloys or different machine optics/spot sizes without retraining on new, material- and machine-specific data. The methodology is transferable, but any practical deployment must respect these domain and machine–material boundaries.

The study concludes that the ML methods, GPR and ANN, are very proficient in predicting hardness in LPBF processes. Furthermore, rollback is a novel method of optimizing output data, which enhanced the metrics of accuracy and was the most appropriate option in this scenario. Future research will focus more on improving prediction accuracy by treating coolant and dresser as independent parameters. The next study to automate the process of smart machining to reach the desired levels of hardness would be to use digitized data through the Industrial Internet of Things (IIoT).

Acknowledgments

This publication is also part of the project PNRR-NGEU which has received funding from the MUR-DM117/2023 for one of the writers (MD), [Project No: MUR DM 117/Tsubaki Nakashima—Recovery, reuse and reduction of waste sludge in the production of balls and rolls for rolling bearings] (November 2023–October 2026), which is gratefully acknowledged. The authors gratefully thank Sophia High Tech (Napoli, Italy), for providing samples for experimental evaluation and for their continuous support in research activities

Funding

Open access funding provided by Politecnico di Torino within the CRUI-CARE Agreement.

References

1. X. Zhang, R. Tiwari, A.H. Shooshtari and M.M. Ohadi, An Additively Manufactured Metallic Manifold-Microchannel Heat Exchanger for High Temperature Applications, *Appl. Therm. Eng.*, 2018, **143**, p 899–908.
2. I. Yadroitsev, I. Yadroitsava, A. Du Plessis and E. MacDonald, *Fundamentals of Laser Powder Bed Fusion of Metals*, Elsevier, 2021
3. Y. Kok, X.P. Tan, P. Wang, M. Nai, N.H. Loh, E. Liu and S.B. Tor, Anisotropy and Heterogeneity of Microstructure and Mechanical Properties in Metal Additive Manufacturing: A Critical Review, *Mater. Des.*, 2018, **139**, p 565–586.
4. P.R. Gradl, S.E. Greene, C. Protz, B. Bullard, J. Buzzell, C. Garcia, J. Wood, R. Osborne, J. Hulka, and K.G. Cooper, Additive Manufacturing of Liquid Rocket Engine Combustion Devices: A Summary of Process Developments and Hot-Fire Testing Results, *2018 Joint Propulsion Conference*, 2018, p 4625
5. S. Soller, R. Behr, S. Beyer, F. Laithier, M. Lehmann, A. Preuss, and R. Salapete, Design and Testing of Liquid Propellant Injectors for Additive Manufacturing, *7th European Conference for Aeronautics and Aerospace Sciences, EUCASS)*, Milano, Italy, 2017
6. D. Liuzzi, C. Boffa, M. Rudnykh, D. Drigo, L. Arione, N. Ierardo and A. Sirbi, Development of an ALM Thrust Chamber for Vega-E M10 Rocket Engine, *Space Propuls.*, 2021, **2020**(1), p 1–8.
7. M. Balbaa, S. Mekhiel, M. Elbestawi and J. McIsaac, On Selective Laser Melting of Inconel 718: Densification, Surface Roughness, and Residual Stresses, *Mater. Des.*, 2020, **193**, p 108818.
8. B. Blakey-Milner, P. Gradl, G. Snedden, M. Brooks, J. Pitot, E. Lopez, M. Leary, F. Berto and A. Du Plessis, Metal Additive Manufacturing in Aerospace: A Review, *Mater. Des.*, 2021, **209**, p 110008.
9. K. Moussaoui, W. Rubio, M. Mousseigne, T. Sultan and F. Rezai, Effects of Selective Laser Melting Additive Manufacturing Parameters of Inconel 718 on Porosity, Microstructure and Mechanical Properties, *Mater. Sci. Eng. A*, 2018, **735**, p 182–190.
10. Y. Li, M. Založnik, J. Zollinger, L. Dembinski and A. Mathieu, Effects of the Powder, Laser Parameters and Surface Conditions on the Molten Pool Formation in the Selective Laser Melting of IN718, *J. Mater. Process. Technol.*, 2021, **289**, p 116930.
11. W.D. Callister and D.G. Rethwisch, *Fundamentals of Materials Science and Engineering*, Wiley, London, 2000
12. R.G. Budynas and J.K. Nisbett, *Shigley's Mechanical Engineering Design*, McGraw-Hill, New York, 2011
13. E. Pavlina and C. Van Tyne, Correlation of Yield Strength and Tensile Strength with Hardness for Steels, *J. Mater. Eng. Perform.*, 2008, **17**, p 888–893.
14. R. Sesana, C. Delprete, M. Pizzarelli, M. Crachi, L. Lavagna, D. Borrelli and A. Caraviello, Influence of Deposition Parameters on Hardness Properties of InconelTM 718 Processed by Laser Powder Bed Fusion for Space Applications, *J. Manuf. Mater. Process.*, 2023, **7**(1), p 36.
15. V. Dovale-Farelo, P. Tavadze, L. Lang, A. Bautista-Hernandez and A. H. Romero, Vickers Hardness Prediction from Machine Learning Methods, *Sci. Rep.*, 2022, **12**(1), p 22475.
16. S. Nasiri and M.R. Khosravani, Machine Learning in Predicting Mechanical behavior of Additively Manufactured Parts, *J. Mater. Res. Technol.*, 2021, **14**, p 1137–1153.
17. P. Charalampous, N. Kladovasilakis, I. Kostavelis, K. Tsongas, D. Tzetzis and D. Tzovaras, Machine Learning-based Mechanical Behavior Optimization of 3D Print Constructs Manufactured via the FFF Process, *J. Mater. Eng. Perform.*, 2022, **31**(6), p 4697–4706.
18. S. Dong, Y. Wang, J. Li, Y. Li, L. Wang and J. Zhang, Machine Learning Aided Prediction and Design for the Mechanical Properties of Magnesium Alloys, *Met. Mater. Int.*, 2024, **30**(3), p 593–606.
19. W. Zhu, W. Huo, S. Wang, Ł Kurpaska, F. Fang, S. Papanikolaou, H. S. Kim and J. Jiang, Machine Learning-based Hardness Prediction of High-Entropy Alloys for Laser Additive Manufacturing, *JOM*, 2023, **75**(12), p 5537–5548.
20. C.L. Mambuscay, C. Ortega-Portilla, J.F. Piamba and M.G. Forero, Predictive Modeling of Vickers Hardness using Machine Learning Techniques on D2 Steel with Various Treatments, *Materials*, 2024, **17**(10), p 2235.
21. U.M.R. Paturi, S.T. Palakurthy, S. Cheruku, B.V. Darshini and N. Reddy, Role of Machine Learning in Additive Manufacturing of Titanium Alloys—A Review, *Arch. Comput. Methods Eng.*, 2023, **30**(8), p 5053–5069.
22. J. Xiong, T. Zhang and S. Shi, Machine Learning of Mechanical Properties of Steels, *Sci. China. Technol. Sci.*, 2020, **63**(7), p 1247–1255.
23. P. Akbari, M. Zamani and A. Mostafaei, Machine Learning Prediction of Mechanical Properties in Metal Additive Manufacturing, *Addit. Manuf.*, 2024, **91**, p 104320.
24. A. Stoll and P. Benner, Machine Learning for Material Characterization with an Application for Predicting Mechanical Properties, *GAMM-Mitt.*, 2021, **44**(1), e202100003
25. Z. Gu, S. Sharma, D.A. Riley, M.V. Pantawane, S.S. Joshi, S. Fu and N.B. Dahotre, A Universal Predictor-based Machine Learning Model for Optimal Process Maps in Laser Powder Bed Fusion Process, *J. Intell. Manuf.*, 2023, **34**(8), p 3341–3363.
26. A. Deka and J. Hall, Predictive Modeling of Mechanical Properties for Fused Deposition Modeling Parts: A Focus on Processing and Environmental Parameters, *Manuf. Lett.*, 2023, **35**, p 643–651.
27. S.D. Grozav, A.D. Sterca, M. Kočiško, M. Pollák and V. Ceclan, Artificial Neural Network-based Predictive Model for Finite Element Analysis of Additive-Manufactured Components, *Machines*, 2023, **11**(5), p 547.
28. Q. Luo, J.D. Shimanek, T.W. Simpson, and A.M. Beese, An Image-based Transfer Learning Approach for using in situ Processing Data to Predict Laser Powder Bed Fusion Additively Manufactured Ti-6Al-4V Mechanical Properties, *3D Printing and Additive Manufacturing*, 2024
29. F. Yan, Y.-C. Chan, A. Saboo, J. Shah, G.B. Olson and W. Chen, Data-Driven Prediction of Mechanical Properties in Support of Rapid Certification of Additively Manufactured Alloys, *Comput. Model. Eng. Sci.*, 2018, **117**(3), p 343–366.
30. M. Banerjee, A. Banerjee, D. Mukherjee, A. Singla, and J. Singh, Machine Learning Module for Predicting Tensile Response of SLMed Ti-6Al-4V, *Advances in Additive Manufacturing and Metal Joining: Proceedings of AIMTDR 2021*, Springer, 2023, p Page
31. V. Maitra and J. Shi, Surface Roughness Prediction for Additively Manufactured Ti-6Al-4V Components Based on Supervised Learning Models, In *International Manufacturing Science and Engineering Conference*, American Society of Mechanical Engineers, 2022, p V001T001A013
32. N.J. van Eck and L. Waltman, VOSviewer: Welcome to VOSviewer, https://www.vosviewer.com/, 2025
33. H. Citakoglu and V. Demir, Developing Numerical Equality to Regional Intensity–Duration–Frequency Curves using Evolutionary Algorithms and Multi-gene Genetic Programming, *Acta Geophys.*, 2023, **71**(1), p 469–488.
34. L. Tonelli, A. Fortunato and L. Ceschini, CoCr Alloy Processed by Selective Laser Melting (SLM): Effect of Laser Energy Density on Microstructure, Surface Morphology, and Hardness, *J. Manuf. Process.*, 2020, **52**, p 106–119.
35. T. DebRoy, H.L. Wei, J.S. Zuback, T. Mukherjee, J.W. Elmer, J.O. Milewski, A.M. Beese, A. Wilson-Heid, A. De and W. Zhang, Additive Manufacturing of Metallic Components–Process, Structure and Properties, *Prog. Mater. Sci.*, 2018, **92**, p 112–224.
36. F. Caiazzo, V. Alfieri and G. Casalino, On the Relevance of Volumetric Energy Density in the Investigation of Inconel 718 laser powder bed fusion, *Materials*, 2020, **13**(3), p 538.
37. M. Skrzyniarz, L. Nowakowski and S. Blasiak, Geometry, Structure and Surface Quality of a Maraging Steel Milling Cutter Printed by Direct Metal Laser Melting, *Materials*, 2022, **15**(3), p 773.
38. R.R. Dehoff, M.M. Kirka, W.J. Sames, H. Bilheux, A.S. Tremsin, L. E. Lowe and S.S. Babu, Site Specific Control of Crystallographic Grain Orientation through Electron Beam Additive Manufacturing, *Mater. Sci. Technol.*, 2015, **31**(8), p 931–938.
39. N.J. Harrison, I. Todd and K. Mumtaz, Reduction of Micro-cracking in Nickel Superalloys Processed by Selective Laser Melting: A Fundamental Alloy Design Approach, *Acta Mater.*, 2015, **94**, p 59–68.
40. Y. Lu, S. Wu, Y. Gan, T. Huang, C. Yang, L. Junjie and J. Lin, Study on the Microstructure, Mechanical Property and Residual Stress of SLM Inconel-718 Alloy Manufactured by Differing Island Scanning Strategy, *Opt. Laser Technol.*, 2015, **75**, p 197–206.
41. E. ISO, Metallic Materials, Vickers Hardness Test. Part 1: Test Method, 2005

42. C. Kuzu, A. Germak, C. Origlia and E. Pelit, Result Analysis of EURAMET Vickers Comparison between INRiM and UME (EURAMET. MH-K1. bc), *Meas. Sens.*, 2021, **18**, p 100268.
43. M.S. Javadi, M.V. Ehteshamfar and H. Adibi, A Comprehensive Analysis and Prediction of the Effect of Groove Shape and Volume Fraction of Multi-walled Carbon Nanotubes on the Polymer 3D-Printed Parts in the Friction Stir Welding Process, *Polym. Test.*, 2023, **117**, p 107844.
44. M.V. Ehteshamfar, M.S. Javadi and H. Adibi, Surface Modification of Prototypes in Fused Deposition Modelling using Lapping Process, *Rapid Prototyp. J.*, 2022, **28**(7), p 1382–1393.
45. M.F. Naqibi, M. Elyasi, H.J. Aval, and M.J. Mirnia, Statistical Modeling and Optimization of Two-Layer Aluminum–Copper Pipe Fabrication by Friction Stir Welding, *Transactions of the Indian Institute of Metals*, 2022, p 1-17
46. F. Aghabeyki, M.J. Mirnia and M. Elyasi, Cold and Warm Flaring of Thin-Walled Titanium Tube using Single-Point Incremental Forming, *Int. J. Adv. Manuf. Technol.*, 2021, **114**(11), p 3357–3376.
47. W.-H. Chen, M.C. Uribe, E.E. Kwon, K.-Y.A. Lin, Y.-K. Park, L. Ding and L.H. Saw, A Comprehensive Review of Thermoelectric Generation Optimization by Statistical Approach: Taguchi Method, Analysis of Variance (ANOVA), and Response Surface Methodology (RSM), *Renew. Sustain. Energy Rev.*, 2022, **169**, p 112917.
48. W. Wu, J. Xue, W. Xu, H. Lin, H. Tang and P. Yao, Parameters Optimization of Auxiliary Gas Process for Double-Wire SS316L Stainless Steel Arc Additive Manufacturing, *Metals*, 2021, **11**(2), p 190.
49. S. Oberloier, W.J. Holmes, L.A. Reich and J.M. Pearce, Particle Swarm Optimization of Printing Parameters for Open-Source TIG-based Metal 3D Printing, *Chin. J. Mech. Eng. Addit. Manuf. Front.*, 2022, **1**(4), p 100050.
50. R.R. Karri and J. Sahu, Modeling and Optimization by Particle Swarm Embedded Neural Network for Adsorption of Zinc (II) by Palm Kernel Shell based Activated Carbon from Aqueous Environment, *J. Environ. Manage.*, 2018, **206**, p 178–191.
51. J. Kennedy and R. Eberhart, Particle Swarm Optimization, *Proceedings of ICNN'95-international conference on neural networks, IEEE*, 1995, p 1942-1948
52. L.C. Cagnina, S.C. Esquivel, and C.A.C. Coello, Solving Engineering Optimization Problems with the Simple Constrained Particle Swarm Optimizer, *Informatica*, 2008, 32(3),
53. M.T. Bhoskar, M.O.K. Kulkarni, M.N.K. Kulkarni, M.S.L. Patekar, G. Kakandikar and V. Nandedkar, Genetic Algorithm and Its Applications to Mechanical Engineering: A Review, *Mater. Today Proc.*, 2015, **2**(4–5), p 2624–2630.
54. P. Potočnik, A. Jeromen and E. Govekar, Genetic Algorithm-based Framework for Optimization of Laser Beam Path in Additive Manufacturing, *Metals*, 2024, **14**(4), p 410.
55. M. Gen and R. Cheng, *Genetic Algorithms and Engineering Optimization*, John Wiley & Sons, 1999
56. G.C. Onwubolu, B. Babu, and K. Deb, Introduction to Genetic Algorithms for Engineering Optimization, *New Optimization Techniques in Engineering*, 2004, p 13-51
57. R. Hassan, B. Cohanim, O. De Weck, and G. Venter, A Comparison of Particle Swarm Optimization and the Genetic Algorithm, In *46th AIAA/ASME/ASCE/AHS/ASC Structures, Structural Dynamics and Materials Conference*, 2005, p 1897
58. C. Wang, D. Li, P. Kaewniam, J. Wang and T. Al Hababi, An ED-PSO Model Updating Algorithm for Structure Health Monitoring of Beam-like Structures, *J. Meas. Eng.*, 2023, **11**(3), p 358–372.
59. M. Jafari, M. Hosseinzadeh and M. Elyasi, Optimization of Tube Drawing Process through FE Analysis, Intelligent Computation, and Experimental Verification, *Proc. Inst. Mech. Eng. E J. Process Mech. Eng.*, 2018, **232**(1), p 94–107.
60. G. Papazoglou and P. Biskas, Review and Comparison of Genetic Algorithm and Particle Swarm Optimization in the Optimal Power Flow Problem, *Energies*, 2023, **16**(3), p 1152.
61. K. Stergiou, C. Ntakolia, P. Varytis, E. Koumoulos, P. Karlsson and S. Moustakidis, Enhancing Property Prediction and Process Optimization in Building Materials through Machine Learning: A Review, *Comput. Mater. Sci.*, 2023, **220**, p 112031.
62. H. Citakoglu, Comparison of Multiple Learning Artificial Intelligence Models for Estimation of Long-Term Monthly Temperatures in Turkey, *Arab. J. Geosci.*, 2021, **14**(20), p 2131.
63. M. Carrasco, J. López and S. Maldonado, Epsilon-Nonparallel Support Vector Regression, *Appl. Intell.*, 2019, **49**(12), p 4223–4236.
64. B. Ghorbani, A. Arulrajah, G. Narsilio and S. Horpibulsuk, Experimental Investigation and Modelling the Deformation Properties of Demolition Wastes Subjected to Freeze–Thaw Cycles using ANN and SVR, *Constr. Build. Mater.*, 2020, **258**, p 119688.
65. G. Yalçın, S. Bayram and H. Çıtakoğlu, Evaluation of Earned Value Management-Based Cost Estimation via Machine Learning, *Buildings*, 2024, **14**(12), p 3772.
66. H. Citakoglu and Ö. Coşkun, Comparison of Hybrid Machine Learning Methods for the Prediction of Short-Term Meteorological Droughts of Sakarya Meteorological Station in Turkey, *Environ. Sci. Pollut. Res.*, 2022, **29**(50), p 75487–75511.
67. E. Schulz, M. Speekenbrink and A. Krause, A tutorial on Gaussian Process Regression: Modelling, Exploring, and Exploiting Functions, *J. Math. Psychol.*, 2018, **85**, p 1–16.
68. M. DehghanpourAbyaneh, P. Narimani, M.S. Javadi, M. Golabchi, S. Attarsharghi and M. Hadad, Predicting Surface Roughness and Grinding Forces in UNS S34700 Steel Grinding: A Machine Learning and Genetic Algorithm Approach to Coolant Effects, *Physchem*, 2024, **4**(4), p 495–523.
69. M. Farid, Data-Driven Method for Real-Time Prediction and Uncertainty Quantification of Fatigue Failure under Stochastic Loading using Artificial Neural Networks and Gaussian Process Regression, *Int. J. Fatigue*, 2022, **155**, p 106415.
70. J. Jenis, J. Ondriga, S. Hrcek, F. Brumercik, M. Cuchor and E. Sadovsky, Engineering Applications of Artificial Intelligence in Mechanical Design and Optimization, *Machines*, 2023, **11**(6), p 577.
71. J. Zhang, P. Wang and R.X. Gao, Deep Learning-based Tensile Strength Prediction in Fused Deposition Modeling, *Comput. Ind.*, 2019, **107**, p 11–21.
72. M.F. Naqibi, M. Elyasi, H.J. Aval and M.J. Mirnia, Statistical Modeling and Optimization of Two-Layer Aluminum–Copper Pipe Fabrication by Friction Stir Welding, *Trans. Indian Inst. Met.*, 2022, **75**(3), p 635–651.
73. P.K. Ambadekar, S. Ambadekar, C. Choudhari, S.A. Patil and S. Gawande, Artificial Intelligence and its Relevance in Mechanical Engineering from Industry 4.0 Perspective, *Aust. J. Mech. Eng.*, 2025, **23**(1), p 110–130.
74. E. Yaghoubi, E. Yaghoubi, A. Khamees and A.H. Vakili, A Systematic Review and Meta-Analysis of Artificial Neural Network, Machine Learning, Deep Learning, and Ensemble Learning Approaches in Field of Geotechnical Engineering, *Neural Comput. Appl.*, 2024, **36**(21), p 12655–12699.
75. A. Kumar and A.K. Ghosh, Decision Tree–and Random Forest–based Novel Unsteady Aerodynamics Modeling using Flight Data, *J. Aircr.*, 2019, **56**(1), p 403–409.
76. Y. Xu, X. Zhao, Y. Chen and Z. Yang, Research on a Mixed Gas Classification Algorithm based on Extreme Random Tree, *Appl. Sci.*, 2019, **9**(9), p 1728.
77. T. Xu, Recent Advances in Rapidly-Exploring Random Tree: A review, *Heliyon*, 2024
78. V. Plevris, G. Solorzano, N.P. Bakas, and M.E.A. Ben Seghier, Investigation of Performance Metrics in Regression Analysis and Machine Learning-based Prediction Models, In *8th European Congress on Computational Methods in Applied Sciences and Engineering (ECCOMAS Congress 2022), European Community on Computational Methods in Applied Sciences*, 2022
79. M. Naser and A.H. Alavi, Error Metrics and Performance Fitness Indicators for Artificial Intelligence and Machine Learning in Engineering and Sciences, *Archit. Struct. Constr.*, 2023, **3**(4), p 499–517.
80. A. Tatachar, L.C. Cole, H.L. Nguyen and K. Heinrich, Evaluation of Pharmacy-based Telephone Interventions on Medication Pick-up Rates: A Retrospective, Quality Improvement Study at Charity Outpatient Clinics, *Int. J. Pharm. Pract.*, 2019, **27**(6), p 510–519.
81. T.O. Hodson, Root Mean Square Error (RMSE) or Mean Absolute Error (MAE): When to use them or not, *Geosci. Model Dev. Discuss.*, 2022, **2022**, p 1–10.
82. D. Chicco, M.J. Warrens and G. Jurman, The Coefficient of Determination R-Squared is more Informative than SMAPE, MAE, MAPE, MSE and RMSE in Regression Analysis Evaluation, *PeerJ Comput. Sci.*, 2021, **7**, e623

83. E.E. Başakın, Ö. Ekmekcioğlu, H. Çıtakoğlu and M. Özger, A New Insight to the Wind Speed Forecasting: Robust Multi-stage Ensemble Soft Computing Approach based on Pre-processing Uncertainty Assessment, *Neural Comput. Appl.*, 2022, **34**(1), p 783–812.
84. T.O. Kvålseth, Cautionary Note about R 2, *Am. Stat.*, 1985, **39**(4), p 279–285.
85. N.J. Nagelkerke, A Note on a General Definition of the Coefficient of Determination, *Biometrika*, 1991, **78**(3), p 691–692.
86. D.C. Montgomery, E.A. Peck and G.G. Vining, *Introduction to Linear Regression Analysis*, Wiley, 2021
87. H. Citakoglu, G. Aktürk and V. Demir, Hybrid Machine Learning for Drought Prediction at Multiple Time Scales: A Case Study of Ağrı Station, Türkiye, *Acta Geophys.*, 2025, **73**(2), p 1643–1677.
88. H.V. Gupta, H. Kling, K.K. Yilmaz and G.F. Martinez, Decomposition of the Mean Squared Error and NSE Performance Criteria: Implications for Improving Hydrological Modelling, *J. Hydrol.*, 2009, **377**(1), p 80–91.
89. K.E. Taylor, Summarizing Multiple Aspects of Model Performance in a Single Diagram, *J. Geophys. Res. Atmos.*, 2001, **106**(D7), p 7183–7192.
90. G.S. Prashanth, P. Sekar, S. Bontha and A. Balan, Grinding Parameters Prediction under Different Cooling Environments using Machine learning Techniques, *Mater. Manuf. Process.*, 2023, **38**(2), p 235–244.
91. Z. Hu, T. Wang, H. Chen, K. Zhang, and H. Wei, Physics-Guided Meta-Learning for Surface Roughness Prediction under Various Working Conditions with Limited Data, *IEEE/ASME Transactions on Mechatronics*, 2025, p 1-11
92. Z. Hu, H. Chen, K. Zhang and H. Wei, Model-based Prediction of Grinding Surface Roughness with Error Correction via a Knowledge-based Fuzzy Broad Learning System, *IEEE Trans. Instrum. Meas.*, 2025, **74**, p 1–14.
93. I. Khan, A. Al Rashid and M. Koç, Integration of Machine Learning and Digital Twin in Additive Manufacturing of Polymeric-based Materials and Products, *Prog. Addit. Manuf.*, 2025, **10**(12), p 10685–10737.
94. W. Huang, J. Yang, H. Yang, G. Jing, Z. Wang and X. Zeng, Heat Treatment of Inconel 718 Produced by Selective Laser Melting: Microstructure and Mechanical Properties, *Mater. Sci. Eng. A*, 2019, **750**, p 98–107.
95. A. Diniță, A. Neacșa, A.I. Portoacă, M. Tănase, C.N. Ilinca and I.N. Ramadan, Additive Manufacturing Post-processing Treatments, A Review with Emphasis on Mechanical Characteristics, *Materials*, 2023, **16**(13), p 4610.
96. M.A. Buhairi, F.M. Foudzi, F.I. Jamhari, A.B. Sulong, N.A.M. Radzuan, N. Muhamad, I.F. Mohamed, A.H. Azman, W.S.W. Harun and M. Al-Furjan, Review on Volumetric Energy Density: Influence on Morphology and Mechanical Properties of Ti6Al4V Manufactured via Laser Powder Bed Fusion, *Prog. Addit. Manuf.*, 2023, **8**(2), p 265–283.
97. S.F. Nabavi, H. Dalir and A. Farshidianfar, A Comprehensive Review of Recent Advances in Laser Powder Bed Fusion Characteristics Modeling: Metallurgical and Defects, *Int. J. Adv. Manuf. Technol.*, 2024, **132**(5), p 2233–2269.
98. J. Liu, H. Ma, L. Meng, H. Yang, C. Yang, S. Ruan, D. Ouyang, S. Mei, L. Deng and J. Chen, Laser Powder Bed Fusion of 316L Stainless Steel: Effect of Laser Polishing on the Surface Morphology and Corrosion Behavior, *Micromachines*, 2023, **14**(4), p 850.
99. J. Heaton, An Empirical Analysis of Feature Engineering for Predictive Modeling, SoutheastCon, *IEEE*, 2016, **2016**, p 1–6.
100. A. Ustundag, M.S. Sivri and K. Menguc, *Feature Engineering, Business Analytics for Professionals*, Springer, 2022